Title

The evolution of whisker-mediated somatosensation in mammals: Sensory processing in barrelless S1 cortex of a marsupial, Monodelphis domestica

Journal

The Journal of Comparative Neurology, 524(17)

ISSN

1550-7149

Authors

Ramamurthy, Deepa L
Krubitzer, Leah A

Publication Date

2016-12-01

DOI

10.1002/cne.24018

Peer reviewed

HHS Public Access

Author manuscript

J Comp Neurol. Author manuscript; available in PMC 2017 December 01.

Published in final edited form as:

J Comp Neurol. 2016 December 1; 524(17): 3587–3613. doi:10.1002/cne.24018.

The evolution of whisker-mediated somatosensation in mammals: sensory processing in barrelless S1 cortex of a marsupial, *Monodelphis domestica*

Deepa L. Ramamurthy[1] and **Leah A. Krubitzer**[1]

[1]Center for Neuroscience, University of California, Davis, Davis CA

Abstract

Movable tactile sensors in the form of whiskers are present in most mammals, but sensory coding in the cortical whisker representation has been studied almost exclusively in mice and rats. Many species that possess whiskers lack the modular "barrel" organization found in the primary somatosensory cortex (S1) of mice and rats, but it is unclear how whisker-related input is represented in these species. We used single-unit extracellular recording techniques to characterize receptive fields and response properties in S1 of *Monodelphis domestica* (short-tailed opossum), a nocturnal, terrestrial marsupial that shared its last common ancestor with placental mammals over 160 million years ago. Short-tailed opossums lack barrels and septa in S1, but show active whisking behavior similar to mice and rats. Most neurons in short-tailed opossum S1 exhibited multiwhisker receptive fields, including a single best whisker and lower magnitude responses to the deflection of surrounding whiskers. Mean tuning width was similar to that reported in mice and rats. Both symmetrical and asymmetrical receptive fields were present. Neurons tuned to ventral whiskers tended to show broad tuning along the rostrocaudal axis. Thus, despite the absence of barrels, most receptive field properties were similar to those reported in mice and rats. However, unlike those species, S1 neuronal responses to best whisker and surround whisker deflection showed comparable latencies in short-tailed opossums. This dissimilarity suggests that some aspects of barrel cortex function may not generalize to tactile processing across mammalian species, and may be related to differences in the architecture of the whisker-to-cortex pathway.

Graphical abstract

[*]**Correspondence to**: Leah A. Krubitzer, University of California, Davis, Center for Neuroscience, 1544 Newton Court, Davis, CA 95618, Phone: 530 757 8560, Fax: 530 757 8827, lakrubitzer@ucdavis.edu.

CONFLICT OF INTEREST STATEMENT

The authors declare that there are no identified conflicts of interest in relation to the current study.

ROLE OF AUTHORS

All authors had full access to all the data in the study and take responsibility for the integrity of the data and the accuracy of the data analysis. Study concept and design: DLR, LAK. Acquisition of data: DLR. Analysis and interpretation of data: DLR, LAK. Drafting of the manuscript: DLR, LAK. Critical revision of the manuscript for important intellectual content: DLR, LAK. Statistical analysis: DLR. Obtained funding: DLR, LAK. Study supervision: LAK.

Barrel-like organization characteristic of mouse and rat S1 is non-ubiquitous among mammals possessing whiskers. In *Monodelphis domestica* S1, which lacks barrels, neurons displayed spatial convergence of whisker inputs, like mouse and rat S1 neurons. Unlike in mice and rats, responses to best vs. surround whisker deflection were not temporally separated.

Keywords

vibrissae; area 3b; receptive fields; barrels; touch; RRID:AB_477329

INTRODUCTION

The emergence of body hair is one of the hallmarks that distinguish mammals from all other extant vertebrate lineages. This evolutionary innovation allowed for the development of a novel class of movable tactile sensors in the form of sinus hairs, or whiskers (also referred to as vibrissae). Present-day mammals use their whiskers for a variety of behavioral functions including the exploration of novel environments, object recognition, spatial navigation, prey capture and social interactions (Mitchinson et al., 2011; Sofroniew et al., 2014; Anjum et. al, 2006; Bobrov et al., 2014; for review see Brecht, 2007; Feldmeyer et al., 2013; Sofroniew and Svoboda, 2015). In fact, whiskers are known to be present at some point during development in nearly all taxa of marsupial and placental mammals (Pocock, 1914; Huber, 1930a; Huber, 1930b; Lyne 1958; Ahl, 1986; Sarko et al., 2011).

The prominent array of long facial whiskers present on the snout, known as the mystacial whiskers, is conserved across mammalian species and displays several species-invariant characteristics in its morphology, including a highly ordered, grid-like arrangement and a systematic variation in both whisker length and shape depending on the position of a whisker within the array (Brecht et al., 1997; Towal et al., 2011). The pattern of innervation of the whisker follicles is similar in marsupial and placental mammals (Patrizi and Munger, 1966; Loo and Halata, 1991; Lee and Woolsey, 1985; Welker and Van der Loos, 1986). In addition, marsupials and placentals share a common bauplan of facial musculature, which involves the muscles typically used to control whisker movement. This muscular arrangement is different from the organization of facial muscles in monotremes, which are

highly derived and do not possess whiskers (Huber, 1930a; Huber, 1930b; Grant et al., 2013). Whisker-mediated somatosensation was therefore likely present in the common ancestor of all marsupial and placental mammals and may have been especially important in exploration and object identification, given the nocturnal lifestyle of our early ancestors (Kemp, 2005; Heesy and Hall, 2010).

The whisker system is a major model for the study of several aspects of cortical function including information encoding and processing, thalamocortical and corticocortical interactions, sensorimotor integration, and active touch sensing (for review see Sofroniew and Svoboda, 2015; Feldmeyer et al., 2013; Diamond et al., 2008; Fox 2008). The discovery of cytoarchitecturally identifiable “barrels,” in layer IV of the primary somatosensory cortex (S1), corresponding to the cortical map of the whiskers in mice (Woolsey and Van der Loos, 1970) and rats (Welker, 1971), combined with the availability of modern genetic and molecular techniques led to the establishment of barrel cortex as an ideal, and widely-used experimental system not only for the study of somatosensory processing, but also for studies of neural circuit development, plasticity and dysfunction.

There are currently over 5,500 extant species of mammals, distributed across 29 different orders, as recorded in the most recent taxonomic compilation of the known species of the world (Roskov et al., 2015). However, a majority of our knowledge regarding the neural circuits that underlie cortical processing stems from the study of only a handful of model species. In particular, despite the ubiquity of whiskers in extant mammalian species, the entire body of research conducted on S1 barrel cortex has created a focus almost exclusively on mice and rats, two closely related genera from the family Muridae, which is just one of 29 families belonging to a single mammalian order, Rodentia (Roskov et al., 2015). As a result, there is an abundance of information on the structural and functional organization of S1 barrel cortex in the mouse and the rat, but little is known about which aspects of barrel cortex organization are derived features specific to murine rodents, and which aspects can be generalized to the neural circuits involved in tactile processing across mammalian species. In the current investigation, we address this dearth of comparative studies on the organization of the whisker representation within the neocortex of mammals by examining the receptive fields and response characteristics of neurons in the S1 whisker representation of short-tailed opossums, *Monodelphis domestica*.

We chose to study this animal model for a number of reasons. First, this is a marsupial that shared its last common ancestor with placental mammals around 160 million years ago (Meredith et al., 2011; O’Leary et al., 2013). Studying the functional organization of S1 in short-tailed opossums, could therefore provide important insights into the features of sensory processing circuits involved in whisker-mediated touch that are common to both marsupial and placental mammals. Second, the peripheral morphology of the whisker array in short-tailed opossums is similar to rats and mice (Grant et al., 2013; Brecht et al., 1997), which implicates the existence of similar constraints, as well as the use of comparable strategies in the sampling and coding of tactile information during whisker-mediated somatosensation. Third, like mice and rats, these opossums exhibit specialized behavior associated with the whiskers known as “whisking”, a stereotypic, rhythmic back-and-forth movement of the facial whiskers during spatial exploration and navigation (Grant et al.,

2013; Mitchinson et al., 2011). Whisking is not present in all animals that possess whiskers; this is an energetically expensive behavior that requires complex, specialized musculature (Huber 1930a; Grant et al., 2013), and is hypothesized to provide a behavioral advantage by increasing the degrees of freedom available for positioning the tactile sensors (Grant et al., 2013).

Finally, there are known structural differences in primary somatosensory cortex of short-tailed opossums, compared to rats and mice. In rats and mice, and some other mammals, histological processing of S1 reveals the presence of a cell-dense, modular cytoarchitecture, the barrels, separated by cell-sparse regions called the septa (Woolsey and Van der Loos, 1970). Neurons in the barrels and septa are known to be associated with distinct thalamocortical and intracortical circuits, and display different receptive field properties (Koralek et al., 1988; Lu and Lin, 1993; Kim and Ebner, 1999; Brecht and Sakmann, 2002; Brecht et al., 2003). Short-tailed opossums, on the other hand, lack any histologically detectable barrels or septa in S1 (Wong and Kaas, 2009; Huffman et al., 1999). This is not an anomaly - many animals that possess whiskers do not have detectable barrels in the cortex (Woolsey et al., 1975), though barrel-like structures may be present at sub-cortical levels, for example, in cats and other carnivores (Nomura et al., 1986), and in water shrews (Catania et al., 2013).

The functional organization of barrel cortex in rats and mice has been described in great detail; there is a precise spatiotopic map of the whisker array in layer IV of S1, such that neurons in each barrel respond primarily to a single best whisker (Welker, 1971; Welker, 1976; Simons, 1978). Neurons also frequently display a much lower magnitude response to other surrounding whiskers (Armstrong-James and Fox, 1987; Welker et al., 1996). Further, there is a clear temporal segregation of the responses to the best whisker and surrounding whiskers, with surround responses having longer latencies than the responses to the best whisker (Armstrong-James and Fox, 1987; Welker et al., 1996). It is unknown whether these receptive field and response properties are features of somatosensory cortex that are also present in other mammals, including those species that naturally lack barrel-like parcellation of S1 whisker cortex.

Therefore, the objective of this study was to quantitatively examine the spatial and temporal response characteristics of single neurons in the S1 whisker representation of short-tailed opossums. By doing so, we aim to elucidate basic features of sensory processing during whisker-mediated touch that are similar or different in marsupial and placental species, with the ultimate goal of identifying common principles of organization of neural circuits in primary somatosensory cortex that can be generalized across all mammalian species.

MATERIALS AND METHODS

Subjects

Eleven adult short-tailed opossums were used in the current study. Nine animals (5 males, 4 females; 85–126 g) were used in electrophysiological recording experiments. Further, one animal was used for additional histology, and another animal was used for Western blot analysis (Figure 1). The animals were housed in standard laboratory cages in which food and

water were available *ad libitum*, and maintained on a 14/10 hour light/dark cycle. All experiments were performed according to the criteria outlined in the National Institutes of Health *Guide for the Care and Use of Laboratory Animals*, and all protocols were approved by the Institutional Animal Care and Use Committee of the University of California, Davis.

Electrophysiological recordings

At the start of the experiment, animals were anesthetized with urethane (1.25 g/kg, 30% in propylene glycol, IP). Supplemental doses of urethane (0.125–0.3125 g/kg, 30% in propylene glycol, IP) were provided if necessary. Respiration and body temperature were monitored throughout the surgery. Animals were given dexamethasone (0.4–2.0 mg/kg, IM) at the beginning of the surgery. Lidocaine (2% solution) was subcutaneously injected at the midline of the scalp and around the ears, and the animal was placed in a stereotaxic frame. An incision was made at the midline of the scalp, the temporal muscle was retracted, and a craniotomy was made such that the parietal cortex was exposed. The head of the animal was stabilized using a skull screw cemented to a head post. The dura was retracted, and the brain was covered with silicone fluid to keep it moist and insulated during the recording session. A digital image was taken of the exposed neocortex so that electrode penetration sites could be directly related to vascular patterns.

Extracellular recordings were made from layer IV (400–500 μm depth below the pial surface) using insulated tungsten microelectrodes (FHC, Inc., Bowdoin, ME; and A–M Systems, Sequim, WA; 1–5 MΩ at 1 kHz). Electrodes were lowered using either a hydraulic microdrive (David Kopf Instruments, Tujunga, CA) or a manually controlled micromanipulator (World Precision Instruments, FL). The location of each recording site was marked on a digital image of the cortical surface relative to the vascular pattern.

Receptive fields were first coarsely mapped using a handheld probe. Following this, if receptive fields were found to be located on the mystacial or genal whisker pad (Figure 2A–D), computer-controlled whisker deflections (see below) were used to quantitatively measure receptive field tuning (Figure 3A–D). Single and multi-unit activity was recorded in response to whisker deflections, and all recorded data were amplified (gain: 10,000X; A–M Systems Model 1800 Microelectrode AC Amplifier; A–M Systems, Carlsborg, WA), streamed as continuous voltage traces sampled at 28 kHz (Power1401, Cambridge Electronic Design Limited, Cambridge, UK) and saved for analysis. Neural activity was monitored through a loudspeaker, and viewed on a computer screen during the experiment. Raw traces were bandpass filtered (300–3000 Hz), and spike-sorting was carried out offline to isolate single units.

At the end of the recording session, fluorescent probes were inserted at specific locations relative to blood vessel landmarks so that electrophysiological recording sites could be related to cortical vasculature and myeloarchitecture. In one case, electrolytic microlesions (10 μA for 10 s) were also placed at known depths to aid in the reconstruction of the laminar and areal positions of recording sites.

Whisker stimulation

At each recording site, neural responses to somatosensory stimulation (consisting of light taps, displacement of whiskers, brushing of skin, hard taps and manipulation of muscles and joints) were tested using a handheld probe. When responses were driven by the deflection of either the mystacial whiskers or the genal whiskers, receptive fields and response properties were quantified as described below.

Whiskers were deflected using computer-controlled piezoelectric actuators (Figure 3A). The piezoelectric device was calibrated using a photodetector circuit (Figure 3B). Whiskers were trimmed to a length of 15 mm. Each individual whisker was inserted into a short, lightweight plastic capillary tube glued to a piezoelectric bimorph element (Q220-AY-203YB, Piezo Systems, Inc., Woburn, MA) fixed on a moveable, jointed arm. The piezoelectric device was positioned such that the whiskers were maintained at their initial resting position and angle. During stimulus presentation, the piezoelectric device was carefully observed under a surgical microscope to ensure that it did not touch the skin or whiskers adjacent to the stimulated whisker.

Stimuli consisted of 2° ramp-hold-return deflections (10 ms ramp, 100 ms hold, 10 ms return; applied 5 mm from the base of the whisker, causing a 1.4 mm excursion of the whisker from its resting position) with an interstimulus interval of 1 or 2 s. For a subset of recording sites, a range of deflection amplitudes (0.1°– 2.0°) was tested to obtain a stimulus strength-response function). Additionally, stimuli with shorter rise/fall times (4 ms ramp, 100 ms hold, 4 ms return) were tested for a subset of recorded neurons. Twelve, twenty-five or fifty trials per stimulus per whisker were collected at each recording site. In order to construct spatial receptive fields, 15–19 neighboring whiskers on the mystacial pad were deflected at every recording site. Except in one animal (for which short whiskers were glued to the capillary tube while being stimulated), receptive fields were not quantified if they were centered on the rostral-most 2–3 mystacial whiskers in Row C and D (Figure 2D), since these whiskers were too short to be held firmly in the piezoelectric device. When a receptive field was located on the genal whiskers, all 7 genal whiskers were tested. For data included in this study, all whisker deflections were made along the rostrocaudal axis.

Histology

Following electrophysiological recording experiments, animals were euthanized with an overdose of sodium pentobarbital (Beuthanasia; 250 mg/kg IP) and transcardially perfused with 0.9% saline, followed by 2–4% paraformaldehyde in phosphate buffer, and then 2–4% paraformaldehyde in 10% phosphate-buffered sucrose. After perfusion, the brain was extracted, and the cortical hemispheres were separated from subcortical structures. The dissected hemispheres were flattened between glass slides, post-fixed briefly in 4% paraformaldehyde in 10% phosphate-buffered sucrose, and then left to soak overnight in 30% sucrose. The flattened cortical hemispheres were sectioned at 30 μm on a freezing microtome. In one case, used exclusively for histology (Figure 4A–C), alternating tangential sections were processed for cytochrome oxidase (Wong-Riley and Welt, 1980; Wong-Riley 1989) and myelin (Gallyas, 1979; Dooley et al, 2013; Figure 4A–C), while in the other cases, myelin staining was used on tangential sections of the neocortex (Figure 5A–C). In

one case, the entire brain was cut coronally into 40 μm sections. Alternating coronal sections were processed for parvalbumin expression (mouse monoclonal anti-parvalbumin from Sigma-Aldrich Co., St. Louis, MO; Cat# P3088, RRID:AB_477329; 1:2000; Wong and Kaas, 2009) or Nissl substance, and used for reconstructing the position of recording sites (Figure 6A–C). When necessary, entire digital images were adjusted for contrast and brightness using Photoshop CS5 (Adobe, San Jose, CA).

Antibody Characterization

We used parvalbumin immunohistochemistry to aid in the identification of areal and laminar boundaries within primary somatosensory cortex in addition to Nissl and myelin staining. Table 2 provides information about the antibody used in the current study. The pattern of parvalbumin expression within short-tailed opossum cortex, was comparable to the patterns previously reported using the same antibody in the same species (Wong and Kaas, 2009). The specificity of this anti-parvalbumin antibody in short-tailed opossums has previously been reported (Olkowicz et al., 2008). We verified these findings by performing Western blot analysis using standard procedures. One animal was deeply anesthetized with isoflurane and decapitated. The brain was then rapidly extracted, and cerebellar hemispheres were dissected out, placed in microcentrifuge tubes, frozen on dry ice, and stored at −80°C until processed. Proteins in the cerebellar tissue lysate were separated using gel electrophoresis. Subsequent to electrophoretic separation, the proteins were transferred from the gel to a membrane, which was removed and incubated overnight at 2–4°C in the primary antibody, MsαParvalbumin (Sigma, P3088), diluted to a concentration of 1:2000 in TBST and 5% NFDM, followed by 1 hour incubation with HRP-conjugated Horse Anti-Mouse IgG Antibody (1:2000, Vector Labs, PI-2000). The resulting protein bands were visualized via ECL detection Clarity Western ECL Substrate (BioRad). As in the previously published study, a single band of labeled protein was clearly visible at around 12 kDa, the molecular weight of parvalbumin (Olkowicz et al., 2008; Figure 1).

Whisker pad processing

In two cases, the whisker pad was processed to visualize the organization of whisker follicles in the mystacial pad and genal areas (Figure 2B–C) (Grant et al., 2013). These portions of the facial skin were removed, shaved, scraped to remove fatty tissues, flattened and dehydrated in a series of ethanol washes with decreasing concentrations of water (50, 70, 95 and 100% ethanol). These were then submerged in xylene until the samples turned clear. The xylene-cleared samples were backlit using a light box and photographed using a Nikon D5100 camera. When necessary, contrast and brightness of entire digital images were adjusted using Photoshop CS5 (Adobe, San Jose, CA).

Data analysis

Single-units were isolated using template-matching procedures, principal component analysis and inspection of interspike interval (ISI) histograms (<0.1% of spikes with ISIs of <1 ms) using Spike2 software (Cambridge Electronic Design Limited, Cambridge, UK). Measurements of spike duration were made from the average spike waveform for each unit. In the current study we did not distinguish between excitatory and inhibitory neurons based on physiological properties; data from neurons with short and long spike durations were

combined for population analyses, since they could not readily be distinguished as distinct populations of neurons based on spike duration alone. Spike times of well-isolated single-units were exported to MATLAB (Mathworks, Inc., Natick, MA) for analysis using custom scripts. Spike trains were aligned to the time of onset of the computer-generated ramp signal, and peristimulus time histograms (PSTHs) were constructed, using a 1 ms bin width (Figure 7A–C, Figure 8A–C). Neural responses were quantified over a 75 ms time window following stimulus onset or offset (Figure 9A–D, Figure 10A–C). Receptive field analysis was performed only for onset responses. Response magnitude was calculated based on the spike count after deflection onset (0–75 ms). Spontaneous firing rates were measured during an equivalent time window during the prestimulus recording period. A neuron was considered to exhibit a significant evoked response if the response magnitude exceeded the prestimulus spike count by more than 2 standard deviations. Neural responses detected using this threshold were in agreement with visual inspection of PSTHs. Only neurons that displayed a significant onset response to at least 1 whisker were included in the remaining analyses. The best whisker (BW) for a neuron was defined as the whisker that evoked the highest response magnitude. Response magnitudes were corrected for spontaneous firing rates. The whiskers at the 8 positions immediately adjacent to the BW (rostral, caudal, dorsal, ventral, rostrodorsal, caudodorsal, rostroventral, caudoventral), are referred to as first-order adjacent whiskers, and the whiskers immediately beyond those are referred to as second-order adjacent whiskers.

Mean receptive fields were constructed after aligning the receptive fields of the individual neurons such that the best whisker was at the center of the receptive field in each case. The response magnitude to the stimulation of each first-order adjacent whisker in the receptive field was normalized by dividing it by the best whisker response magnitude. Contour plots (generated after smoothing the response magnitude matrix by linear interpolation) were used to visualize individual, as well as mean receptive fields (Figure 11A–E, Figure 12A–D). The *tuning width index* for each neuron was calculated as the mean response to stimulation of the first-order adjacent whiskers divided by the best whisker response (Figure 12E). Higher tuning width indices indicate broader receptive fields. In case a whisker was absent at any of the first-order whisker positions, those values were considered to be missing, and means were calculated without including those values. This was necessary since there are only 5 positions (out of 25) in the short-tailed opossum mystacial whisker pad (B1, B2, C1, C2, C3), at which whiskers are present at all 8 adjacent positions, and we did not restrict data collection to neurons that had their BWs at those 5 positions. The mean receptive field was also separately computed for the subset of neurons (7/70neurons) for which surrounding whiskers were tested at all 8 positions immediately adjacent to the BW. In addition to the overall tuning width index, a row tuning width index calculated as the mean response of the adjacent whiskers in the same row as the BW (in-row surround whiskers), divided by the BW response and an arc tuning width index calculated as the mean response of the two adjacent whiskers in the same arc as the BW (in-arc surround whiskers), divided by the BW response were also calculated. These were used to calculate the *shape index* for each neuron, defined as the difference between the row tuning width index and the arc tuning width index, divided by their sum (Figure 12F, Figure 13A–D). In cases where the sum of the row and arc tuning width indices was zero, the shape index was assigned to be zero. Shape index values

range from −1 to 1, with positive values indicating broader tuning along the row compared to the arc, and negative values indicating broader tuning along the arc compared to the row.

Population average PSTHs (Figure 14A) were smoothed with a 3 ms moving average for the purpose of visualization. Latency measures were computed based on unsmoothed PSTHs. All latency values are reported relative to the onset of movement of the piezoelectric device. Two measures of response latency (Figure 14A–G) were used when significant evoked responses were observed: (1) onset latency (time of occurrence of the first 1 ms bin of the PSTH that contains a firing rate greater than 2 standard deviations above spontaneous firing) and (2) peak latency (the time of the 1 ms bin of the PSTH that contained the maximum number of spikes). Statistical analyses were performed in MATLAB version 8.1.0 (Mathworks, Inc., Natick, MA) and R version 3.2.0 (R Development Core Team 2015). Summary data are reported as mean ± standard error of the mean (SEM). Kolmogorov–Smirnov test was used to compare firing rate distributions. For each parameter, normality of the distribution was assessed using the Shapiro-Wilks test. Two sample t-tests were used to compare population means, and paired sample t-tests were used to make comparisons for paired data. Whenever assumptions of normality were not met, statistical analyses were repeated using non-parametric tests (Wilcoxon rank-sum test to compare population medians, and Wilcoxon signed-rank test for matched pair comparisons). Bonferroni's correction was used when multiple comparisons were made. A non-parametric multivariate analysis of variance (MANOVA) was used to check for influences of sex and individual differences on response magnitude, onset latency, peak latency, tuning width index, and shape index. Differences were considered to be statistically significant when $p<0.05$.

RESULTS

The primary objective of this study was to quantitatively characterize the receptive fields and response properties of single neurons in the primary somatosensory cortex (S1) of short-tailed opossums. Across 9 animals, we made extracellular recordings of neural activity from 107 single units, in response to the computer-controlled deflection of individual whiskers. 15–19 neighboring mystacial whiskers or all 7 genal whiskers were tested for each unit. 70/107 units exhibited a significant evoked response to the deflection of at least one mystacial or genal whisker, and these were used in the analyses of the spatial and temporal response characteristics of neurons in S1. A summary of the sampling of responsive neurons is provided in Table 3. For the parameters examined (see *Methods*), no statistically significant differences were found between sexes or among animals, so all data were combined for analysis.

Whisker pad morphology

In *Monodelphis domestica*, the large facial whiskers are arranged in a grid-like pattern consisting of horizontal rows and vertical arcs, with an overall organization that is similar to rats and mice. Direct comparisons between the whisker pad morphology of short-tailed opossums and other mammals, including rats and mice, have been made in previous studies (Grant et al., 2013, Brecht et al., 1997). In addition to the mystacial whiskers on the snout (23 per side), short-tailed opossums also possess a set of genal whiskers (5–10 per side) in

the cheek region, that are absent in rats and mice, but are present in all examined species of marsupials (Lyne, 1958) (Figure 2A–D). Facial whiskers are also present at supraorbital, interramal and submental positions in short-tailed opossums, but are generally less prominent, and were not investigated in the current study. We visualized the arrangement of the mystacial and genal whiskers in short-tailed opossums using an ethanol/xylene cleared preparation of the whisker pads (Figure 2B–C) as previously described by Grant and colleagues (2013), in order to get a clear depiction of the peripheral morphology of the whisker system. The nomenclature used in this study to refer to specific whiskers is adapted from Grant and colleagues (2013). The mystacial whiskers in short-tailed opossums are arranged in a well-defined grid of 4 rows (A-D, dorsal to ventral), and 6 arcs (0–6, caudal to rostral), along with 2 straddler whiskers (α and β) located on either side of row B (Figure 2B, D). The mystacial whiskers were highly stereotypical in their number and placement on the snout. The dorsal two rows of mystacial whiskers had fewer whiskers (three in row A, four in row B) than the ventral two rows (seven each in row C and row D). The α whisker is situated between rows A and B, and the β whisker is situated between rows C and D. In general, mystacial whiskers increased in size (diameter and length) from rostral to caudal positions, and from dorsal to ventral positions. Two nasal whiskers (NV1 and NV2) are located dorsal to the mystacial whiskers, and several small sinus hairs constituting the furry buccal pad (FBP) are located ventral to the mystacial whiskers. The genal whiskers are arranged in 1–2 arcs [G and H; 0–5, or higher indices (see below), dorsal to ventral] on the cheek (Figure 2C, D). Though always present as a vertically arranged group in the cheek region, the genal whiskers showed inter-individual variability in number and position, unlike the stereotypically arranged mystacial whiskers. For consistency, the genal whisker at the most dorsal position was considered to be the G1 whisker, and remaining genal whiskers were identified based on their position relative to this whisker.

We examined the responses of neurons in S1 to stimuli that were applied to the mystacial as well as genal whiskers. Quantitative data were not collected when receptive fields were centered on the rostral-most 2–3 mystacial whiskers in the C-row and the D-row, since those whiskers were too short to be secured in the piezoelectric actuator device. Apart from that, we did not restrict data collection to neurons that had their receptive fields on any specific portion of the whisker array.

Qualitative assessment of receptive fields

For every recording site, a handheld probe was first used to qualitatively assess receptive fields while monitoring unit activity using an oscilloscope and audio monitor. Neural responses were tested for the deflection of all mystacial and genal whiskers on both ipsilateral and contralateral sides, as well as the skin and fur on the snout in the region adjacent to, and in between the whiskers. For neurons that responded to whisker deflection, responses were only evoked by whiskers on the contralateral side; stimulation of ipsilateral whiskers and adjacent skin and fur failed to evoke detectable responses under our recording conditions. Mystacial and genal whiskers did not, in any case, evoke responses in the same neurons. At some sites, evoked responses could only be detected in response to the deflection of a single whisker while at other sites, multiple whiskers were found to elicit a response. When a receptive field was found to span more than one whisker, it was often

difficult to localize a single whisker within the receptive field that evoked the greatest magnitude of response, because 2–3 neighboring whiskers evoked responses that were qualitatively similar.

Architecture of the S1 whisker region in *Monodelphis domestica*

Previous studies have examined the architectural structure of the primary somatosensory cortex (area 3b or S1) in the short-tailed opossum using a variety of immunocytochemical and histological techniques (Wong and Kaas, 2009; Huffman et al., 1999). These studies have been unable to demonstrate the presence of distinct barrel fields or barrel-like subdivisions in these animals, unlike rodents like rats and mice, or marsupials like the brush-tailed possum, the striped possum and the tammar wallaby (Woolsey et al., 1975; Weller, 1993; Huffman et al., 1999; Waite et al., 1991). Consistent with these previous studies, we found that cytochrome oxidase histochemistry, a technique which allows for the visualization of cortical barrel fields (Wong-Riley and Welt, 1980), failed to reveal barrel-like organization within the architectural boundaries of primary somatosensory cortex (Figure 4A–C). We further verified this lack of barrels by recording from the S1 whisker region in short-tailed opossums, and directly relating the locations of electrophysiological recording sites with the myeloarchitecture and cytoarchitecture of primary somatosensory cortex.

The relationship of electrophysiological recording sites to the architectural borders of S1 was determined by reconstructing tangential sections of the flattened cortex, stained for myelin. Primary sensory areas, including S1, in short-tailed opossums were densely myelinated and darkly stained compared to surrounding cortical areas (Figure 5A–B) (Catania et al., 2000; Wong and Kaas, 2009; Dooley et al., 2013). Fluorescent probes were used to reconstruct the positions of electrode penetrations. Neurons that responded to the deflection of whiskers were located laterally in S1 (Figure 5C), in correspondence with the location of the S1 whisker representation in somatotopic body maps of short-tailed opossums previously determined using microelectrode multi-unit mapping techniques (Catania et al., 2000; Dooley et al., 2013). Myelin staining was uniformly dark in the region of the S1 whisker representation throughout all cortical layers, with no visible heterogeneities indicative of barrel-like organization. The relationship of electrophysiological recording sites to the laminar borders of S1 was determined by reconstructing coronal sections of the cortex, stained in alternate series for parvalbumin (Figure 6A) and Nissl substance (Figure 6B). Layer IV of S1 stains darkly for parvalbumin-immunopositive terminals, along with several parvalbumin-immunopositive cell bodies (Wong and Kaas, 2009). Layer IV of S1 is also very well-defined in Nissl-stained sections, appearing as a darkly stained band containing densely packed cell bodies (Wong and Kaas, 2009; Karlen and Krubitzer, 2007). A microlesion used to mark the position of a recording site in the S1 whisker representation is indicated in Figure 6A–C. Cytoarchitectural parcellation into barrel fields or barrel-like subdivisions cannot be detected in the S1 whisker region, using either parvalbumin or Nissl-staining.

Quantitative measurement of receptive fields

Whenever hand-mapping indicated an evoked response to at least one whisker, receptive fields and response characteristics of the neuron were quantitatively measured using computer-controlled ramp-hold-return stimuli (Figure 3A–D). Receptive fields were measured by recording the activity of single neurons in response to the deflection of individual whiskers. Typically, neurons responded maximally to the deflection of a single whisker (best whisker, BW), but also responded with a lower magnitude to multiple surrounding whiskers. For all recorded neurons (n =107), responses to the stimulation of the BW were measured, as well as to the stimulation of an additional 14–18 mystacial whiskers and 6–7 genal whiskers, so that the spatial receptive field measurements were as complete as possible. Figures 6 and 7 show examples of the responses of neurons in S1 to the computer-controlled deflection of individual whiskers. In the first example, the neuron has its receptive field on the mystacial whiskers, and responds with the highest magnitude to the deflection of the D0 whisker (Figure 7A–C). In addition, deflection of two surrounding whiskers D1 and D2 also evoked significant neural responses; the D1 response was 65.0% of the D0 response while the D2 response was 44.5% of the D0 response. In the second example, the neuron has its receptive field on the genal whiskers and responds with the highest magnitude to the deflection of the G6 whisker (Figure 8A–C), while deflection of four surrounding whiskers G5, G4, G3, and G2 produced significant neural responses that were 90.5%, 76.2%, 42.9% and 14.3%, respectively, of the G6 response. Except for the example shown in Figure 8, for which the receptive field was present on the genal whiskers, all the remaining responsive neurons (n = 69 neurons) in our dataset had their receptive fields on the mystacial whiskers.

Spontaneous and evoked activity

When deflections with amplitudes ranging from 0.1° to 2.0° were applied to the BWs of individual neurons, these neurons displayed monotonically increasing stimulus strength-response functions (Figure 9A). Response magnitudes rapidly increase between 0.1° and 0.5° (mean: 0.1 ± 0.1 spikes/stimulus at 0.1°, 1.3 ± 0.2 spikes/stimulus at 0.5°), and on average begin to saturate at amplitudes higher than 0.5° (mean: 1.8 ± 0.2 spikes/stimulus at 2.0°). However, in some cases response magnitudes continued to increase between 1.5° and 2.0° (the two highest amplitudes for which neural responses were measured). For receptive field analyses, 2.0° deflections were used in all cases to maximize the recorded evoked response, while maintaining an amplitude of deflection for which there was no detectable mechanical stimulation of whiskers, fur and skin adjacent to the whisker held in the piezoelectric device.

In our dataset, 49% (52/107) of neurons displayed a significant evoked response following stimulus onset alone, 17% (18/107) of neurons displayed a significant evoked response following both stimulus onset and offset, and 0% (0/107) of neurons displayed a significant evoked response following stimulus offset alone (Figure 9B). The spontaneous firing rate was low (mean: 0.6 ± 0.2 spikes/s; median: 0.2 ± 0.3). Onset period firing rates were significantly different from spontaneous firing rates (mean: 13.3 ± 1.8 spikes/s; two sample t-test, $p<0.001$; median: 9.0 ± 2.3 spikes/s; Wilcoxon rank-sum test, $p<0.001$). Offset period firing rates were lower than onset period firing rates (mean: 7.0 ± 2.3 spikes/s; two sample t-test, $p<0.05$; median: 3.1 ± 2.9 Wilcoxon rank sum test, $p<0.05$), but significantly different

from spontaneous firing rates (two sample t-test, $p<0.001$; Wilcoxon rank sum test, $p<0.001$) (Figure 9C). For the data included in receptive field analyses (onset responsive neurons, n =70), the distributions of onset period firing rates and offset period firing rates were both significantly different from the spontaneous firing rate distribution (Figure 9D), and from each other (two-sample Kolmogorov-Smirnov test, $p < 0.001$ in all cases). Subsequent analyses were restricted to the neurons that evoked a significant onset response (data corresponding to the black and gray bars in Figure 9B–C); receptive field properties of offset responses were not analyzed in the current study.

Receptive field size

To characterize the extent of the whisker array that elicited a response in individual neurons, receptive field size was first measured as the number of whiskers that evoked a significant response above spontaneous activity, and ranged in size from 1 to 14 whiskers (Figure 10A). Median receptive field size for the population of recorded S1 neurons was 3.0 whiskers (mean receptive field size: 3.7). Among all responsive neurons, 31% (22/70) responded only to a single best whisker, while the remaining neurons also responded to the deflection of multiple neighboring whiskers, in addition to the BW. Most responsive neurons (87%; 61/70) had a receptive field size of 7 or fewer whiskers. In more than half the dataset (64%; 45/70) two or more whiskers in the receptive field elicited a firing rate greater than 50% of the response evoked by the BW (Figure 10B). However, the average first-order adjacent whisker response was ~25% of the BW response, suggesting that overall tuning was narrow (Figure 10C). There was a further decrease in the response magnitude to <15% of the BW magnitude, at the second-order adjacent whisker positions.

Spatial configuration of receptive fields

Receptive fields were visualized using contour plots (Figure 11A–E). The aim of this analysis was not to get a depiction of the entire receptive field (which, as noted above, could include anywhere between 1 and 14 whiskers), but rather to examine the spatial configuration of the receptive field at positions immediately surrounding the BW, assuming that the BW is the center of the receptive field (see *Methods* for further details). The majority of receptive fields were oval or round (80%; 56/70) (Figure 11A–C; based on 50% response level), but more irregular shapes (20%; 14/70) were also observed (Figure 11D–E; based on 50% response level).

The mean receptive field for single neurons in the S1 whisker representation of short-tailed opossums was calculated by averaging the spatial receptive fields, consisting of the BW and eight immediately adjacent surrounding whiskers, across all neurons (Figure 12A–B). The mean evoked response at all eight surrounding whisker positions was less than 50% of the BW response, with the highest mean evoked response of 39% ± 4% at the rostroventral position, and the lowest mean evoked response of 15% ± 5%, at the dorsal position. Due to the morphology of the short-tailed opossum whisker pad (Figure 2A–D), surrounding whiskers were not present at all eight positions for all recorded units (see *Methods* for details). Therefore, the mean receptive field was also calculated separately for the neurons (n = 7) in which surrounding whiskers were present at all eight positions. Again, the mean

surround whisker evoked response was less than 50% of the BW response at all 8 positions, ranging from 1 ± 1% to 12 ± 9% (Figure 12C–D).

A tuning width index was calculated for each neuron as the ratio of the mean responses evoked by surrounding whiskers at the immediately adjacent positions, to the response evoked by the BW. Overall, receptive fields were narrowly tuned (Figure 12E; mean tuning width index: 0.25 ± 0.03; median tuning width index: 0.24 ± 0.04). Tuning width index was significantly positively correlated ($r = 0.55$, $p<0.05$) for pairs of units that were recorded within the same penetration. Though on average 2–3 whiskers in each receptive field evoked greater than 50% of the BW response (Figure 10B), mean surround values at all 8 immediate surround whisker positions was <50% of the BW response (Figure 12A–D). The dominant surround whisker (second best whisker; SBW) was not consistently located at any specific surround position. In the neurons that displayed a significant response to at least 2 whiskers (n = 48/70), SBW and BW could be located in the same row (52%; 25/48) or different rows (48%; 23/48). Also, SBW could be located rostral to BW (44%; 21/48), caudal to BW (46%; 22/48) or in the same arc as BW (10%; 5/48).

To assess the symmetry of tuning, a shape index was calculated for each neuron by measuring the tuning width index separately for in-row surrounding whiskers and the in-arc surrounding whiskers, and then computing a contrast index using those values (see *Methods*). Symmetrically tuned neurons, defined as those with a shape index between −0.2 and +0.2, made up 36% (25/70) of sites, while the remaining displayed asymmetrical tuning, with the receptive field skewed along either the row or the arc. More neurons had strongly skewed receptive fields (shape index less than −0.6 or greater than +0.6) along the BW row (31%; 22/70) than the BW arc (11%; 8/70). Median shape index was 0.00 ± 0.09, while mean shape index was 0.20 ± 0.07, indicating that the average receptive field was symmetrical, with a slight trend towards broader row tuning in the population. Shape index exhibited a weak trend towards positive correlation between pairs of units from the same recording penetration ($r = 0.14$, $p>0.05$).

Tuning differences based on best whisker position

We observed that a larger proportion of neurons in our dataset responded maximally to whiskers located in the D-row of the mystacial pad (57%; 39/69), compared to all the other rows combined (43%; 30/69) (Figure 13A). Though this could either be due to a sampling bias in the location of the recording sites in our experiments or due to a true magnification of the representation of the D-row whiskers in S1, we were interested in testing whether there were any systematic differences in the tuning of neurons that had their BWs in the D-row, compared to those neurons that had their BWs in the other three rows.

In general, the D-row group of neurons had row tuning width indices that were higher than their arc tuning width indices (Figure 13B), while a trend in the opposite direction was seen for the non D-row group of neurons. There was no significant difference in the tuning width indices of the two groups (two-tailed two-sample t-test, $p>0.05$; Wilcoxon rank sum test, $p>0.05$; Figure 13C), suggesting that the average response evoked by the surrounding whiskers relative to the BW was similar in both groups. However, shape index for the D-row group of neurons was significantly higher than the non D-row group of neurons (two-tailed

two-sample t-test, $p<0.001$; Wilcoxon rank sum test, $p<0.01$; Figure 13D). This indicates asymmetric tuning in the D-row group of neurons, with the in-row surround whiskers evoking a higher firing rate than the in-arc surround whiskers, on average. In contrast, non D-row whiskers were more likely to be asymmetrical along either axis, with a bias towards being elongated along the arc.

Temporal response characteristics

We examined the temporal characteristics of single neurons in S1 in response to the deflection of the best whisker and the surrounding whiskers. S1 neurons responded to best whisker deflection at short latencies, with the earliest responses occurring at <10 ms (Figure 14, Table 4). In the neurons that displayed a significant response to at least 2 whiskers (n = 48), we compared the temporal characteristics of the neural response to the deflection of the best whisker (BW), and the second-best whisker (SBW; the dominant surround whisker) by examining the population average peristimulus time histograms (Figure 14A). The average population neural activity exhibited a similar time course in response to BW and SBW deflection. The onset component of the PSTHs also displays similar firing rates for both BW and SBW deflection. The distribution of response magnitudes of the SBW relative to the BW demonstrates that in a majority of cases, the SBW evokes a response that is greater than 50% of the BW response (mean: 74.9% ± 2%; median: 79.4 ± 3%; Figure 14B) However, paired comparisons of the firing rate during the onset period (0–75 ms) show that there is a significant difference between the response evoked by the BW and the response evoked by the SBW (two-tailed paired sample t-test, $p<0.001$; Wilcoxon signed-rank test; $p<0.001$; Figure 14C). Interestingly, the offset component of the neural response displays a trend towards higher average firing rates in response to SBW deflection, compared to BW deflection.

We compared the latencies of the response to BW and SBW deflection, for the onset response, as well as the peak of the response. Onset latency differences between BW and SBW responses were centered around zero (Figure 14D; mean: 1.7 ± 1.4 ms, median: 0.0 ± 1.7 ms). Pairwise comparisons between BW and SBW onset latencies were not significantly different (Figure 14E; two-tailed paired sample t-test, $p>0.05$; Wilcoxon signed-rank test, $p>0.05$). Thus, cortical neurons begin to respond to either BW or SBW deflection at similar times following the stimulus. In comparison with onset latency differences, the distribution of peak latency differences between BW and SBW responses was shifted towards positive values (Figure 14F; mean: 3.2 ± 1.7 ms, median: 3.5 ± 2.1 ms). However, pairwise comparisons between BW and SBW peak latencies were not significantly different (Figure 14G; two-tailed paired sample t-test, $p>0.05$; Wilcoxon signed-rank test, $p>0.05$). These results suggest that neural responses evoked by best whisker and surround whisker deflection exhibit a low level of temporal segregation, if any, in layer IV of short-tailed opossum S1.

In a subset of neurons (23/107), we measured BW and SBW response magnitudes and latencies for stimuli with 10 ms ramps, as well as 4 ms ramps (see *Methods*). Summary data are listed in Table 4. For neurons which exhibited a significant response to the stimulation of at least two whiskers (n = 16), the parameters quantifying the relationship between SBW and

BW responses (relative response magnitude, onset latency difference, peak latency difference) were not significantly different for 4 ms ramp stimuli compared to 10 ms ramp stimuli (two-tailed paired sample t-test, $p>0.05$; Wilcoxon signed-rank test, $p>0.05$, in all cases).

DISCUSSION

Numerous studies have used electrophysiological recording techniques to qualitatively examine the functional organization of the somatosensory cortex in a variety of mammals including species of monotremes (Krubitzer et al, 1995), marsupials (Huffman et al., 1999; Catania et al, 2000; Frost et al., 2000; for review, see Karlen and Krubitzer, 2007) and placentals (for review see Jones and Peters, 1990). These comparative studies have provided important insights into the evolution of cortical fields in mammals, and the relationship between cortical organization and specializations in peripheral morphology and behavior. Different morphological features are specialized for tactile behavior in different mammalian species; examples include the bill of a platypus (Krubitzer et al., 1995), the nasal star of a star-nosed mole (Catania et al., 1993), the forepaw of a raccoon (Welker and Seidenstein, 1959), the incisors of a naked mole rat (Catania and Remple, 2002), the whiskers of a rat (Welker 1971), and the hand of a primate (Nelson et al., 1980). In each of these cases, there is an expansion of the representation of the behaviorally relevant body surface within S1. The proportion of S1 dedicated to representing the whiskers in short-tailed opossums (~20%; based on data from Catania et al., 2000) is similar to that in rats (20%; Welker 1971), underscoring the importance of whiskers as a tactile sensory array in short-tailed opossums (*Monodelphis domestica*).

We characterized the spatial and temporal response properties of neurons in the whisker representation of the primary somatosensory cortex of the short-tailed opossum. This is the first investigation of receptive fields and response properties of neurons in the whisker representation in an animal that naturally lacks histologically detectable barrels and septa in S1, but uses its whiskers in a manner similar to rats and mice. Additionally, this is the first study to quantify receptive field characteristics of neurons in the somatosensory cortex of a non-eutherian mammal.

This comparative analysis of receptive field organization can provide insights into critical features of cortical circuits in mammals that have emerged for the processing of distinct sensory inputs, and for the facilitation of touch-mediated detection and discrimination using specialized sensory effector organs. We focused on characterizing responses of neurons in layer IV, since this is the main thalamorecipient layer in mammalian sensory cortex, and the spatial and temporal aspects of receptive field organization can be expected to affect subsequent processing in other cortical layers of S1, as well as higher-order cortical areas.

We first discuss our findings on receptive field sizes in the opossum S1 whisker representation in comparison with other mammalian species. We then address anisotropies and whisker-specific differences we observed in our data, and compare these results to literature available on the barrel cortex of mice and rats. Finally, we address the differences in spatial and temporal processing in opossums, compared to rats and mice, as well as

certain strains of mutant mice that exhibit a barrelless cytoarchitectural phenotype in S1 similar to what is naturally observed in the short-tailed opossum.

Spatial convergence of whisker inputs

Receptive fields of single neurons in the S1 whisker representation have been well defined in rats and mice (Armstrong-James and Fox 1987; Armstrong-James et al., 1992; Petersen and Sakmann 2001; Brecht and Sakmann 2002, Quairiaux et al., 2007; Li et al, 2009). Since the sensory array in the whisker system consists of a punctate distribution of receptors associated with a grid-like layout of sinus hairs, we first quantified receptive field sizes in terms of the total number of whiskers that evoked a significant response in S1 neurons. Reported values of mean receptive field size in rats have ranged from 1.58 (under fentanyl anesthesia; Simons and Carvell 1989) to 8 whiskers (under barbiturate anesthesia; Waite and Taylor 1978).

As noted by Fox (2008), these receptive field estimates were likely influenced by a number of factors including: type of anesthesia and anesthetic depth, behavioral state (arousal and attention levels), type of stimulus applied (single-whisker vs. multiwhisker stimuli, temporal dynamics of stimuli), method of neural response detection (qualitative vs. quantitative), and definition of the neural response (threshold used to discriminate spontaneous vs. driven neural activity. We used urethane anesthesia, which is now commonly used for acute neurophysiological recording in rodents due to the stability of the anesthetic state that can be achieved (Niell and Stryker, 2008). Under these conditions, our estimate of the receptive field size (mean: 3.7 whiskers; median: 3.0 whiskers) was in good agreement with receptive field sizes reported for layer IV neurons in urethane-anesthetized rats (mean: 3.2 whiskers, Ito 1985; 4.0 whiskers, Armstrong-James and Fox 1987). Most neurons in short-tailed opossum S1 exhibited multiwhisker receptive fields, responding predominantly to a single best whisker, but also displaying a lower magnitude response to the deflection of surrounding whiskers. Thirty-one percent of S1 neurons displayed single-whisker receptive fields, similar to the proportion in layer IV of rodent barrel cortex (31%, Ito, 1985; 29%, Fox et al., 2003).

To date, quantitative estimations of receptive field sizes of single neurons in the S1 whisker representation have not been obtained in any studies of non-rodent species. However, qualitative assessments of receptive field size from studies that focused on other aspects of neuronal responses are available in a few other species of placental mammals, namely rabbits, cats and shrews.

In studies aimed at examining direction selectivity of the best whisker, receptive field sizes of inhibitory interneurons in layer IV of rabbit S1 were qualitatively assessed (55% of which were observed to have single whisker receptive fields in awake rabbits; Swadlow 1989; Alonso et al., 2005; Swadlow and Gusev 2002). However, the mean tuning width of S1 neurons in the current study was closer to mean tuning width of regular-spiking excitatory neurons in mice (Gabernet et al., 2005) suggesting that our dataset was dominated by excitatory neurons. Therefore, our data cannot be compared directly with available data from the rabbit barrel cortex. In S1 of cats, single neurons were observed to have multiwhisker receptive fields with a gradient-like organization (Schultz et al, 1976; Fomovskii, 1980).

Thirty-nine percent of neurons in cat S1 responded to only a single whisker (qualitative assessment under barbiturate anesthesia; Schultz, 1976).

Receptive fields of multiunit activity combined across different lamina in S1 were reported in one study on the cortical organization in the Etruscan shrew (*Suncus etruscus*), a nocturnal, insectivorous tactile specialist that uses its whiskers to hunt prey (Roth-Alpermann et al., 2010; Anjum et al., 2006). The mean receptive field size in shrew S1, measured under urethane anesthesia, was 10 whiskers. This is much larger than receptive fields in S1 in rodents and short-tailed opossums using the same anesthetic, however it is difficult to make direct comparisons with our data for a few reasons: first, the shrew data are based on multiunit activity, which could lead to larger estimates of receptive field size; and second, quantitatively assessed data were obtained only in one animal (though this estimate was reportedly consistent with hand-mapping data of multiunit whisker receptive fields obtained in additional experiments).

Receptive fields have been measured in the S1 representations of a few other specialized touch systems in mammals, like the nasal star in star-nosed moles and the hands of primates. A majority of receptive fields in single neurons in the S1 star representation were confined to a single star appendage (average RF size<1 square mm; Sachdev and Catania, 2002). Similarly, in the S1 (area 3b) hand representation of rhesus macaques, single neuron receptive fields were mostly confined to a single digit (average RF size = 14 square mm; DiCarlo et al., 1998).

In all species that have been examined to date, neurons in the S1 whisker representation respond to the deflection of more than one whisker, that is, there is convergence of sensory inputs across multiple whiskers. However, the morphology of the sensory apparatus in the whisker system is very different than the nasal star (Sachdev and Catania, 2002) or the hand. An individual whisker deflection comprises a point-like stimulus on the sensory epithelium. In contrast, each appendage of the star and each digit of the primate hand has a large, continuous surface area that is covered by several touch receptors. Due to these differences in the peripheral morphologies it is difficult to make direct comparisons of the spatial convergence of inputs in the whisker system with other specialized touch systems in mammals.

Asymmetries in spatial tuning of neurons

Prior reports of the spatial tuning of neurons in layer IV of barrel cortex in mice and rats have mostly found small, symmetrical receptive fields compared to neurons in other cortical layers (Welker et al, 1993; Armstrong-James and Fox, 1987; Chapin 1986). However, in these studies, asymmetry of tuning was not quantified for individual neurons – it was either reported qualitatively, or quantitatively from the mean receptive fields after averaging across all neurons. The mean receptive field for our dataset (Figure 12A–B) indicated a relative response magnitude of less than 50% of the best whisker response at all first-order adjacent whisker positions, similar to layer IV neurons in mice (Welker et al, 1993), but a slight elongation of the receptive field along the row-axis was observed (apparent in the contour plot, Figure 12A). In order to examine the distribution of receptive field shapes across the dataset, we quantified the tuning shape of receptive fields of neurons in the S1 whisker

representation in the short-tailed opossum using a continuous variable, the shape index (see *Methods*, for further details). Using this method, we found a substantial proportion of neurons with highly symmetric receptive fields (36%) in layer IV of S1, consistent with previous studies. However, we also found that 40% of the neurons were highly asymmetrically tuned along either the row (31%) or the arc (11%), with a bias towards neurons more broadly tuned along the row.

This is in agreement with reports of anisotropic anatomical and functional organization in barrel cortex of mice and rats, which displays a bias towards integration of inputs from whiskers within the same row, rather than those from different rows. S1 barrel columns corresponding to the same row of whiskers are more similar to each other in terms of neuronal numbers, compared to barrel columns corresponding to whiskers in different rows (Meyer et al., 2013). In mice, barrel columns representing whiskers within the same row are more highly interconnected than those belonging to different rows (Bernardo et al., 1990). Voltage sensitive dye imaging and electrophysiological recordings in barrel cortex of rats have demonstrated that single whisker stimulation initially evokes responses in the barrel column corresponding to the stimulated whisker, but the responses subsequently spread across the barrel cortex, with preferential activation of barrel columns within the same row (Lustig et al., 2013; Armstrong-James and Fox, 1987). Additionally, in rats, S1 barrels within the same row show higher levels of overlap of projection zones in other cortical areas (S2 and M1) compared to barrels representing different rows of whiskers (Hoffer et al., 2003).

Thus, a common feature of receptive field shape, in the few species that have been studied, is an elongation within a row of whiskers. Systematic biases towards asymmetries along any specific axes have not been found in the receptive fields for neurons in the hand representation in rhesus macaques (DiCarlo et al, 1998). This might be due to the differences in the morphology of the peripheral effectors involved. The hand has a continuous sheet of touch receptors and is used to manipulate objects, in addition to performing tactile detection and discrimination. In contrast, the whisker array, which consists of a punctate distribution of receptors associated with a grid of whiskers, is swept across objects in a stereotypic manner. Since whisking primarily involves movements along the rostro-caudal axis, parallel to the whisker rows, whiskers within any given row are more likely to be stimulated together or in sequence, during the natural behavior of the animal. Therefore, integration of inputs from different whiskers within a row could facilitate the detection of the location and tactile features of objects in the environment.

Whisker-specific differences in neuronal tuning

We found differences in the receptive field organization of neurons that were tuned to whiskers in the D-row, the ventral-most row of the mystacial array in short-tailed opossums, compared to neurons that were tuned to whiskers in rows A–C. Specifically, though there was no overall difference in tuning width, neurons with receptive fields on D-row whiskers were more broadly tuned along the row axis compared to the arc axis, resulting in more asymmetric receptive fields in these neurons. In contrast, neurons with receptive fields on

whiskers in more dorsal rows had a tendency to be more broadly tuned along the arc axis, rather than the row axis.

These results are consistent with reports of row-specific differences in the structural and functional organization of barrel cortex in rodents. Meyer and colleagues (2013) used high-resolution confocal imaging to reconstruct the cellular architecture of S1 barrel columns corresponding to different whiskers in the rat, and found that there were significant differences in the structural organization of the barrel columns corresponding to different whiskers. The total number of neurons within each cortical barrel column increased from the most dorsal row of mystacial whiskers (A-row) to the most ventral row of mystacial whiskers (E-row). Additionally, there were whisker-specific differences in the laminar organization of the cortex, in the barrel columns corresponding to the ventral rows of mystacial whiskers, compared to those corresponding to the dorsal rows of whiskers. There is some evidence that these architectural differences among barrel columns corresponding to different whisker rows may be correlated with differences in functional organization. A different study found that in rat barrel cortex, layer IV neurons in E-row barrel columns displayed a stronger tendency to be preferentially activated by adjacent whiskers in the same row, compared to neurons in the C-row and D-row barrel columns which display less of a row-preference (Armstrong-James and Fox, 1987).

In our study, neurons tuned to whiskers in the upper rows (A–C) displayed broader tuning along the arc, suggesting that there are high levels of connectivity between the representations of dorsal rows of whiskers with the ventral rows of whiskers. This corroborates studies of intracortical connections in mice that show preferential connectivity of the barrel columns of the small, dorsal whiskers with the large barrel columns of the E-row, in addition to being well-connected with other small barrel columns.

Given the three-dimensional morphology of the whisker array in mammals, with whisker-specific differences in the shape, size and orientation, which depend on the position of the whisker in the array (Towal et al., 2011; Brecht et al., 1997), the fact that there are differences in the cortical organization corresponding to different whiskers is not surprising, though these differences have not been well explored. Ventral whisker rows are, in general, larger and more numerous than the dorsal whiskers, which could explain differences in neuronal numbers and cortical thickness of the associated barrel columns. Differences in tuning could be attributed to differences in the behavioral use of whiskers in the ventral rows compared to the dorsal rows since the ventral rows are closer to the ground during locomotion. For neurons that are tuned to whiskers in the ventral-most row (D-row in opossums; E-row in mice and rats), broader tuning along the row could potentially facilitate the detection of obstacles or inconsistencies in the animal’s path, or vibrations in the ground. The behavioral relevance of these ventral row whiskers could lead to a magnification of their representation in the cortex, which could explain the over-representation of neurons tuned to the D-row in our dataset. Over-representation of specific portions of specialized sensory effector arrays has been previously reported in the somatosensory system. For example, in the star-nosed mole, there is a magnification of the representation of the star in the S1 somatotopic map. Additionally, the 11th appendage of the star, which acts as a tactile fovea

during foraging, is highly over-represented within the S1 star representation (see Catania, 2012, for review).

These studies, including the present work, that show whisker-specific differences in thalamic and cortical organization are counter to the notion that S1 cortex is comprised of repeating, identical stereotypic units. Studies of receptive field organization and plasticity in mice and rats are frequently limited to neurons within specific barrel columns, usually C2 or D2, since the corresponding principal and adjacent whiskers can most easily be accessed for controlled stimulation. While further work is necessary to directly link the whisker-specific differences in functional organization to differences in the structural organization of barrel columns, the existence of such whisker-specific differences should be considered in the interpretation of studies that are limited to individual barrel columns.

Temporal convergence of whisker inputs

The functional organization of barrel cortex in rats and mice is closely linked to its modular anatomy - there is a precise spatiotopic map of whiskers in layer IV of S1 in which neurons in each barrel respond primarily to a single best whisker (Welker, 1971; Armstrong-James and Fox, 1987). Neurons also respond to whiskers surrounding the best principal whisker, but there is a spatial and temporal segregation of the responses to the best whisker and the surrounding whiskers, with neurons having much longer latencies (5–30 ms delay; Armstrong-James and Fox, 1987; Armstrong-James and Callahan, 1991; Welker et al, 1993; Welker et al., 1996) when responding to stimulation of surround whiskers compared to stimulation of the best whisker, in addition to having much lower response magnitudes (20–30% of the best whisker response, Armstrong-James and Fox, 1987; Welker et al., 1996). The existence of these temporal differences in the responses of single neurons to different whiskers has led to the proposition that the timing of the neural response, in addition to the spike count, can encode information about the spatial location of a stimulus (Panzeri et al., 2001). In short-tailed opossums, we found that the dominant surround whisker evoked high magnitude responses (>70% BW response), with no significant delay relative to the best whisker. This suggests that timing differences in neural responses to the stimulation of different whiskers may not play a role in encoding stimulus location in short-tailed opossums. These interspecies differences in relative response latencies could be related to increased convergence of inputs at the sub-cortical or cortical levels in short-tailed opossums, compared to mice and rats, or due to differences in the connections of inhibitory circuits.

Neural response properties have been previously examined in a few different strains of mutant mice which exhibit a barrelless phenotype in S1 cortex. In *brl* mice (adenylyl cyclase 1 loss-of-function mutants) there is an absence of barrel-like clustering of layer IV neurons, as well as a lack of segregation of thalamocortical arbors in S1 (Welker et al., 1996; Abdel-Majid et al, 1998; Gheorghita et al, 2006). In these mice, surround whiskers evoked high-magnitude responses (>50% BW response) with very little delay following the best whisker response (2.5 ms on average, compared to an average of 13.5 ms in normal animals; Welker et al., 1996). Similarly, a lack of temporal segregation of best whisker and dominant surround whisker responses was reported in mGluR5 knockout mice, which lack layer IV

cell clustering but retain thalamocortical arbor segregation in a portion of the S1 whisker representation (She et al, 2009). These findings, which are similar to our results in short-tailed opossums, suggest that discrete barrels may be part of an architecture that creates a latency difference in best whisker and surround whisker input. However, temporal segregation of best whisker and surround whisker responses was present in Tg8 mice (monoamine oxidase A knockout mutants), which lack both layer IV cell clusters and thalamocortical arbor segregation (Yang et al, 2001). Tg8 mice display normal whisker-related pattering at subcortical levels (Cases et al., 1996), unlike *brl* mice which display more poorly defined barreloids in the thalamic ventrobasal nucleus, compared to normal animals (Welker et al., 1996). This suggests that relative latency differences in best whisker and surround whisker input may not be directly related to modular organization at the level of the cortex, and but could be associated with segregation of whisker inputs at subcortical levels. Previous studies in short-tailed opossums (Olkowicz et al., 2008) have noted the absence of visible parcellation in the ventrobasal nucleus of the thalamus; parcellation in the trigeminal brainstem has not been examined to date. However, visualization of barreloids can require sectioning of the thalamus at angles that are oblique to standard cutting planes (Haidarliu and Ahissar, 2001). Further, segmentation in both cortical and subcortical structures may be more clearly identified in juvenile brain tissue compared to adult brain tissue (Catania et al., 2013; Haidarliu and Ahissar, 2001). Therefore, to have a good understanding of parcellation of the whisker-to-cortex pathway in short-tailed opossums, it would be important to conduct a more thorough examination of cortical and subcortical structures, over the course of development. It is plausible that in animals possessing a modular organization of barrel cortex, this type of architectural structure, and the accompanying microcircuitry, optimizes tactile discrimination by enhancing spatiotemporal segregation of the neural response to different whisker inputs. If so, differences in the architectural structure of S1 may be reflective of the tactile capabilities of different species. However, it is possible that animals that naturally do not possess barrels in whisker cortex, rather than being functionally impaired, use different and possibly simpler, circuits and information encoding strategies for whisker-mediated touch sensation. In this case, studying rodents in comparison to a phylogenetically distant species like *Monodelphis domestica*, could help us understand aspects of cortical processing that are shared across mammalian species.

Evolution of whisker-mediated somatosensation in mammals

The prevalence of whiskers among extant mammals and the similarities in their structure and function in phylogenetically distant taxa, rodents and marsupials, suggest that this is an evolutionarily old system. The early common ancestors of therian mammals (marsupials and placentals) were likely nocturnal (Gerkema et al., 2013), and therefore may have relied heavily on the use of their whiskers to perform functions like exploration and navigation, which would later be taken over by the visual system in diurnal mammals. While many more comparative studies are necessary to come to firm conclusions about the cortical organization of the whisker system in these early mammals, a few common themes can be observed based on the available data, providing insights into shared features of cortical processing in mammals. At the early stages of cortical somatosensory processing there is a large proportion of small, symmetrical receptive fields, which could be involved in

performing fine tactile discriminations. However, the majority of neurons in layer IV respond to the stimulation of multiple whiskers, indicating the convergence of excitatory inputs across whiskers. This allows for integration of information across sensory receptors and would thereby favor the detection of tactile stimuli in the environment. In whisker-mediated somatosensation, there is a preferential integration of inputs along the horizontal rows of whiskers, coincident with the caudorostral sweep of the whiskers during whisking. Further, similar to other sensory systems, stimuli that impinge upon different portions of the sensory receptor arrays are represented differently in the cortex. In the whisker system, there appears to be an over-representation of the ventral-most row of mystacial whiskers; a row which contains the largest whiskers. This is combined with differences in neuronal tuning such that there is a higher level of row-wise convergence of inputs in neurons tuned to ventral whiskers, in comparison with the neurons tuned to whiskers in dorsal rows. This is consistent with the ventral whisker rows being more likely to come in contact with obstacles or inconsistencies in the path of the animal.

Thus, the similarities in the peripheral morphology and use of the whisker system in rodents and marsupials are accompanied by a number of similarities in sensory processing of whisker inputs at the level of the cortex. These similarities are likely reflective of somatosensory neural circuits that emerged early in the course of mammalian evolution. The possession of a new tactile sensory specialization in the form of the whisker system would have conferred an adaptive advantage for a nocturnal lifestyle, and therefore, played an important role in the survival of early, ancestral mammals.

Acknowledgments

OTHER ACKNOWLEDGEMENTS

We are grateful to Dr. Daniel E. Feldman and Dr. Gregg H. Recanzone for many helpful discussions, and for comments on a draft of this manuscript. We thank Cynthia Weller, Rebecca Hao and Dr. Brian Trainor for providing expertise and resources for western blot analysis, and Dr. Mary Baldwin for histological assistance and helpful suggestions regarding this paper. Many thanks also to Dr. Dylan Cooke, Dr. James Dooley and Dr. Adam Goldring for critically reading the manuscript, Dr. Jeffrey Johnson for programming assistance, Dr. Cindy Clayton for animal care, Adam Gordon, Raquel Valdes, and Krisha Yadav-Rajan for experimental assistance.

This research was supported by NIH NEI R01EY022987-01 to LAK, NIH NEI 2T32EY015387-11 and NSF GRFP DGE-1148897 to DLR.

LITERATURE CITED

Abdel-Majid RM, Leong WL, Schalkwyk LC, Smallman DS, Wong ST, Storm DR, Fine A, Dobson MJ, Guernsey DL, Neumann PE. Loss of adenylyl cyclase I activity disrupts patterning of mouse somatosensory cortex. Nat Genet. 1998; 19(3):289–291. [PubMed: 9662407]

Anjum F, Turni H, Mulder PG, van der Burg J, Brecht M. Tactile guidance of prey capture in Etruscan shrews. Proc Natl Acad Sci U S A. 2006; 103(44):16544–16549. [PubMed: 17060642]

Ahl AS. The role of vibrissae in behavior: a status review. Vet Res Commun. 1986; 10(4):245–268. [PubMed: 3526705]

Alonso JM, Swadlow HA. Thalamocortical specificity and the synthesis of sensory cortical receptive fields. J Neurophysiol. 2005; 94(1):26–32. [PubMed: 15985693]

Armstrong-James M, Fox K. Spatiotemporal convergence and divergence in the rat S1 “barrel” cortex. J Comp Neurol. 1987; 263(2):265–281. [PubMed: 3667981]

Armstrong-James M, Callahan CA. Thalamo-cortical processing of vibrissal information in the rat. II. spatiotemporal convergence in the thalamic ventroposterior medial nucleus (VPm) and its relevance to generation of receptive fields of S1 cortical “barrel” neurones. J Comp Neurol. 1991; 303(2):211–224. [PubMed: 2013636]

Armstrong-James M, Fox K, Das-Gupta A. Flow of excitation within rat barrel cortex on striking a single vibrissa. J Neurophysiol. 1992; 68(4):1345–1358. [PubMed: 1432088]

Bernardo KL, McCasland JS, Woolsey TA, Strominger RN. Local intra- and interlaminar connections in mouse barrel cortex. J Comp Neurol. 1990; 291(2):231–255. [PubMed: 2298933]

Brecht M. Barrel cortex and whisker-mediated behaviors. Curr Opin Neurobiol. 2007; 17(4):408–416. [PubMed: 17702566]

Brecht M, Naumann R, Anjum F, Wolfe J, Munz M, Mende C, Roth-Alpermann C. The neurobiology of Etruscan shrew active touch. Philos Trans R Soc Lond B Biol Sci. 2011; 366(1581):3026–3036. [PubMed: 21969684]

Brecht M, Preilowski B, Merzenich MM. Functional architecture of the mystacial vibrissae. Behavioural Brain Research. 1997; 84(1–2):81–97. [PubMed: 9079775]

Brecht M, Roth A, Sakmann B. Dynamic receptive fields of reconstructed pyramidal cells in layers 3 and 2 of rat somatosensory barrel cortex. J Physiol. 2003; 553(Pt 1):243–265. [PubMed: 12949232]

Brecht M, Sakmann B. Dynamic representation of whisker deflection by synaptic potentials in spiny stellate and pyramidal cells in the barrels and septa of layer 4 rat somatosensory cortex. J Physiol. 2002; 543(Pt 1):49–70. [PubMed: 12181281]

Bobrov E, Wolfe J, Rao RP, Brecht M. The representation of social facial touch in rat barrel cortex. Curr Biol. 2014; 24(1):109–115. [PubMed: 24361064]

Catania KC. Evolution of brains and behavior for optimal foraging: a tale of two predators. Proc Natl Acad Sci U S A. 2012; 109(Suppl 1):10701–10708. [PubMed: 22723352]

Catania KC, Northcutt RG, Kaas JH, Beck PD. Nose stars and brain stripes. Nature. 1993; 364(6437): 493. [PubMed: 8336790]

Catania KC, Catania EH, Sawyer EK, Leitch DB. Barrelettes without barrels in the American water shrew. PLoS One. 2013; 8(6):e65975. [PubMed: 23755296]

Catania KC, Jain N, Franca JG, Volchan E, Kaas JH. The organization of somatosensory cortex in the short-tailed opossum (Monodelphis domestica). Somatosens Mot Res. 2000; 17(1):39–51. [PubMed: 10833083]

Catania KC, Remple MS. Somatosensory cortex dominated by the representation of teeth in the naked mole-rat brain. Proc Natl Acad Sci U S A. 2002; 99(8):5692–5697. [PubMed: 11943853]

Catania KC, Catania EH, Sawyer EK, Leitch DB. Barrelettes without Barrels in the American Water Shrew. PLoS ONE. 2013; 8(6):e65975. [PubMed: 23755296]

Chapin JK. Laminar differences in sizes, shapes, and response profiles of cutaneous receptive fields in the rat SI cortex. Exp Brain Res. 1986; 62(3):549–559. [PubMed: 3720884]

Diamond ME, von Heimendahl M, Knutsen PM, Kleinfeld D, Ahissar E. ‘Where’ and ‘what’ in the whisker sensorimotor system. Nat Rev Neurosci. 2008; 9(8):601–612. [PubMed: 18641667]

DiCarlo JJ, Johnson KO, Hsiao SS. Structure of receptive fields in area 3b of primary somatosensory cortex in the alert monkey. J Neurosci. 1998; 18(7):2626–2645. [PubMed: 9502821]

Dooley JC, Franca JG, Seelke AM, Cooke DF, Krubitzer LA. A connection to the past: Monodelphis domestica provides insight into the organization and connectivity of the brains of early mammals. J Comp Neurol. 2013; 521(17):3877–3897. [PubMed: 23784751]

Dooley JC, Franca JG, Seelke AM, Cooke DF, Krubitzer LA. Evolution of mammalian sensorimotor cortex: thalamic projections to parietal cortical areas in Monodelphis domestica. Front Neuroanat. 2014; 8:163. [PubMed: 25620915]

Fomovskii BI. Somatosensory cortical unit responses to stimulation of the vibrissae in cats. Neurophysiology. 1980; 12(2):85–90.

Fox, K.; Woolsey, T. Barrel Cortex. Cambridge University Press; 2008.

Fox K, Wright N, Wallace H, Glazewski S. The origin of cortical surround receptive fields studied in the barrel cortex. J Neurosci. 2003; 23(23):8380–8391. [PubMed: 12968000]

Frost SB, Milliken GW, Plautz EJ, Masterton RB, Nudo RJ. Somatosensory and motor representations in cerebral cortex of a primitive mammal (Monodelphis domestica): a window into the early evolution of sensorimotor cortex. J Comp Neurol. 2000; 421(1):29–51. [PubMed: 10813771]

Gabernet L, Jadhav SP, Feldman DE, Carandini M, Scanziani M. Somatosensory integration controlled by dynamic thalamocortical feed-forward inhibition. Neuron. 2005; 48(2):315–327. [PubMed: 16242411]

Feldmeyer D, Brecht M, Helmchen F, Petersen CC, Poulet JF, Staiger JF, Luhmann HJ, Schwarz C. Barrel cortex function. Prog Neurobiol. 2013; 103:3–27. [PubMed: 23195880]

Gallyas F. Silver staining of myelin by means of physical development. Neurol Res. 1979; 1(2):203–209. [PubMed: 95356]

Gerkema MP, Davies WIL, Foster RG, Menaker M, Hut RA. The nocturnal bottleneck and the evolution of activity patterns in mammals. Proceedings of the Royal Society of London B: Biological Sciences. 2013; 280:1765.

Grant RA, Haidarliu S, Kennerley NJ, Prescott TJ. The evolution of active vibrissal sensing in mammals: evidence from vibrissal musculature and function in the marsupial opossum Monodelphis domestica. J Exp Biol. 2013; 216(Pt 18):3483–3494. [PubMed: 23737559]

Haidarliu S, Ahissar E. Size gradients of barreloids in the rat thalamus. J Comp Neurol. 2001; 429(3): 372–387. [PubMed: 11116226]

Heesy CP, Hall MI. The nocturnal bottleneck and the evolution of mammalian vision. Brain Behav Evol. 2010; 75(3):195–203. [PubMed: 20733295]

Hoffer ZS, Hoover JE, Alloway KD. Sensorimotor corticocortical projections from rat barrel cortex have an anisotropic organization that facilitates integration of inputs from whiskers in the same row. J Comp Neurol. 2003; 466(4):525–544. [PubMed: 14566947]

Huber E. Evolution of Facial Musculature and Cutaneous Field of Trigeminus. Part I. The Quarterly Review of Biology. 1930a; 5(2):133–188.

Huber E. Evolution of Facial Musculature and Cutaneous Field of Trigeminus. Part II. The Quarterly Review of Biology. 1930b; 5(4):389–437.

Huffman KJ, Nelson J, Clarey J, Krubitzer L. Organization of somatosensory cortex in three species of marsupials, Dasyurus hallucatus, Dactylopsila trivirgata, and Monodelphis domestica: neural correlates of morphological specializations. J Comp Neurol. 1999; 403(1):5–32. [PubMed: 10075440]

Ito M. Processing of vibrissa sensory information within the rat neocortex. Journal of Neurophysiology. 1985; 54(3):479–490. [PubMed: 4045535]

Jones, EG.; Peters, A. Cerebral Cortex: Comparative Structure and Evolution of Cerebral Cortex. Springer US; 2012.

Karlen SJ, Krubitzer L. The functional and anatomical organization of marsupial neocortex: evidence for parallel evolution across mammals. Prog Neurobiol. 2007; 82(3):122–141. [PubMed: 17507143]

Kemp, TS. The origin and evolution of mammals. Oxford University Press; 2005.

Kim U, Ebner FF. Barrels and septa: separate circuits in rat barrels field cortex. J Comp Neurol. 1999; 408(4):489–505. [PubMed: 10340500]

Koralek KA, Jensen KF, Killackey HP. Evidence for two complementary patterns of thalamic input to the rat somatosensory cortex. Brain Res. 1988; 463(2):346–351. [PubMed: 2461788]

Krubitzer L, Manger P, Pettigrew J, Calford M. Organization of somatosensory cortex in monotremes: in search of the prototypical plan. J Comp Neurol. 1995; 351(2):261–306. [PubMed: 7699113]

Lee KJ, Woolsey TA. A proportional relationship between peripheral innervation density and cortical neuron number in the somatosensory system of the mouse. Brain Res. 1975; 99(2):349–353. [PubMed: 1182550]

Li L, Bender KJ, Drew PJ, Jadhav SP, Sylwestrak E, Feldman DE. Endocannabinoid signaling is required for development and critical period plasticity of the whisker map in somatosensory cortex. Neuron. 2009; 64(4):537–549. [PubMed: 19945395]

Loo SK, Halata Z. Innervation of hairs in the facial skin of marsupial mammals. J Anat. 1991; 174:207–219. [PubMed: 2032935]

Lu SM, Lin RC. Thalamic afferents of the rat barrel cortex: a light- and electron-microscopic study using Phaseolus vulgaris leucoagglutinin as an anterograde tracer. Somatosens Mot Res. 1993; 10(1):1–16. [PubMed: 8484292]

Lustig BR, Friedman RM, Winberry JE, Ebner FF, Roe AW. Voltage-sensitive dye imaging reveals shifting spatiotemporal spread of whisker-induced activity in rat barrel cortex. J Neurophysiol. 2013; 109(9):2382–2392. [PubMed: 23390314]

Lyne AG. The Systematic and Adaptive Significance of the Vibrissae in the Marsupialia. Proceedings of the Zoological Society of London. 1959; 133(1):79–133.

Meredith RW, Janecka JE, Gatesy J, Ryder OA, Fisher CA, Teeling EC, Goodbla A, Eizirik E, Simao TL, Stadler T, Rabosky DL, Honeycutt RL, Flynn JJ, Ingram CM, Steiner C, Williams TL, Robinson TJ, Burk-Herrick A, Westerman M, Ayoub NA, Springer MS, Murphy WJ. Impacts of the Cretaceous Terrestrial Revolution and KPg extinction on mammal diversification. Science. 2011; 334(6055):521–524. [PubMed: 21940861]

Meyer HS, Egger R, Guest JM, Foerster R, Reissl S, Oberlaender M. Cellular organization of cortical barrel columns is whisker-specific. Proc Natl Acad Sci U S A. 2013; 110(47):19113–19118. [PubMed: 24101458]

Mitchinson B, Grant RA, Arkley K, Rankov V, Perkon I, Prescott TJ. Active vibrissal sensing in rodents and marsupials. Philos Trans R Soc Lond B Biol Sci. 2011; 366(1581):3037–3048. [PubMed: 21969685]

Naumann RK, Anjum F, Roth-Alpermann C, Brecht M. Cytoarchitecture, areas, and neuron numbers of the Etruscan shrew cortex. J Comp Neurol. 2012; 520(11):2512–2530. [PubMed: 22252518]

Niell CM, Stryker MP. Highly selective receptive fields in mouse visual cortex. J Neurosci. 2008; 28(30):7520–7536. [PubMed: 18650330]

Nelson RJ, Sur M, Felleman DJ, Kaas JH. Representations of the body surface in postcentral parietal cortex of Macaca fascicularis. J Comp Neurol. 1980; 192(4):611–643. [PubMed: 7419747]

Nomura S, Itoh K, Sugimoto T, Yasui Y, Kamiya H, Mizuno N. Mystacial vibrissae representation within the trigeminal sensory nuclei of the cat. J Comp Neurol. 1986; 253(1):121–133. [PubMed: 2432098]

O'Leary MA, Bloch JI, Flynn JJ, Gaudin TJ, Giallombardo A, Giannini NP, Goldberg SL, Kraatz BP, Luo ZX, Meng J, Ni X, Novacek MJ, Perini FA, Randall ZS, Rougier GW, Sargis EJ, Silcox MT, Simmons NB, Spaulding M, Velazco PM, Weksler M, Wible JR, Cirranello AL. The placental mammal ancestor and the post-K-Pg radiation of placentals. Science. 2013; 339(6120):662–667. [PubMed: 23393258]

Olkowicz S, Turlejski K, Bartkowska K, Wielkopolska E, Djavadian RL. Thalamic nuclei in the opossum Monodelphis domestica. J Chem Neuroanat. 2008; 36(2):85–97. [PubMed: 18571895]

Panzeri S, Petersen RS, Schultz SR, Lebedev M, Diamond ME. The Role of Spike Timing in the Coding of Stimulus Location in Rat Somatosensory Cortex. Neuron. 2001; 29(3):769–777. [PubMed: 11301035]

Patrizi G, Munger BL. The ultrastructure and innervation of rat vibrissae. J Comp Neurol. 1966; 126(3):423–435. [PubMed: 5937260]

Petersen CC, Sakmann B. Functionally independent columns of rat somatosensory barrel cortex revealed with voltage-sensitive dye imaging. J Neurosci. 2001; 21(21):8435–8446. [PubMed: 11606632]

Pocock, R. 48. On the Facial Vibrissæ of Mammalia. Wiley Online Library; 1914. p. 889-912.

Quairiaux C, Armstrong-James M, Welker E. Modified sensory processing in the barrel cortex of the adult mouse after chronic whisker stimulation. J Neurophysiol. 2007; 97(3):2130–2147. [PubMed: 17122325]

Roskov Y, Abucay L, Orrell T, Nicolson D, Kunze T, Culham A, Bailly N, Kirk P, Bourgoin T, DeWalt RE, Decock W, De Wever A. Species 2000 & ITIS Catalogue of Life, 2015 Annual Checklist. 2015 Digital resource at www.catalogueoflife.org/annual-checklist/2015. Species 2000: Naturalis, Leiden, the Netherlands. ISSN 2405-884X.

Roth-Alpermann C, Anjum F, Naumann R, Brecht M. Cortical organization in the Etruscan shrew (Suncus etruscus). J Neurophysiol. 2010; 104(5):2389–2406. [PubMed: 20668271]

Sachdev RN, Catania KC. Receptive fields and response properties of neurons in the star-nosed mole's somatosensory fovea. J Neurophysiol. 2002; 87(5):2602–2611. [PubMed: 11976396]

Sarko DK, Rice FL, Reep RL. Mammalian tactile hair: divergence from a limited distribution. Ann N Y Acad Sci. 2011; 1225:90–100. [PubMed: 21534996]

Schultz W, Galbraith GC, Gottschaldt KM, Creutzfeldt OD. A comparison of primary afferent and cortical neurone activity coding sinus hair movements in the cat. Exp Brain Res. 1976; 24(4):365–381. [PubMed: 1261624]

Simons DJ. Response properties of vibrissa units in rat SI somatosensory neocortex. J Neurophysiol. 1978; 41(3):798–820. [PubMed: 660231]

Simons DJ, Carvell GE. Thalamocortical response transformation in the rat vibrissa/barrel system. J Neurophysiol. 1989; 61(2):311–330. [PubMed: 2918357]

She WC, Quairiaux C, Albright MJ, Wang YC, Sanchez DE, Chang PS, Welker E, Lu HC. Roles of mGluR5 in synaptic function and plasticity of the mouse thalamocortical pathway. Eur J Neurosci. 2009; 29(7):1379–1396. [PubMed: 19519626]

Sofroniew NJ, Cohen JD, Lee AK, Svoboda K. Natural whisker-guided behavior by head-fixed mice in tactile virtual reality. J Neurosci. 2014; 34(29):9537–9550. [PubMed: 25031397]

Swadlow HA. Efferent neurons and suspected interneurons in S-1 vibrissa cortex of the awake rabbit: receptive fields and axonal properties. J Neurophysiol. 1989; 62(1):288–308. [PubMed: 2754479]

Swadlow HA, Gusev AG. Receptive-field construction in cortical inhibitory interneurons. Nat Neurosci. 2002; 5(5):403–404. [PubMed: 11967546]

Towal RB, Quist BW, Gopal V, Solomon JH, Hartmann MJ. The morphology of the rat vibrissal array: a model for quantifying spatiotemporal patterns of whisker-object contact. PLoS Comput Biol. 2011; 7(4):e1001120. [PubMed: 21490724]

Waite PM, Marotte LR, Mark RF. Development of whisker representation in the cortex of the tammar wallaby Macropus eugenii. Brain Res Dev Brain Res. 1991; 58(1):35–41. [PubMed: 2015652]

Waite PM, Taylor PK. Removal of whiskers in young rats causes functional changes in cerebral cortex. Nature. 1978; 274(5671):600–602. [PubMed: 672993]

Welker C. Microelectrode delineation of fine grain somatotopic organization of SmI cerebral neocortex in albino rat. Brain Research. 1971; 26(2):259–275. [PubMed: 4100672]

Welker C. Receptive fields of barrels in the somatosensory neocortex of the rat. J Comp Neurol. 1976; 166(2):173–189. [PubMed: 770516]

Welker WI, Seidenstein S. Somatic sensory representation in the cerebral cortex of the racoon (Procyon lotor). The Journal of Comparative Neurology. 1959; 111(3):469–501. [PubMed: 13843838]

Welker E, Van der Loos H. Quantitative correlation between barrel-field size and the sensory innervation of the whiskerpad: a comparative study in six strains of mice bred for different patterns of mystacial vibrissae. J Neurosci. 1986; 6(11):3355–3373. [PubMed: 3772437]

Welker E, Armstrong-James M, Van der Loos H, Kraftsik R. The mode of activation of a barrel column: response properties of single units in the somatosensory cortex of the mouse upon whisker deflection. Eur J Neurosci. 1993; 5(6):691–712. [PubMed: 8261141]

Welker E, Armstrong-James M, Bronchti G, Ourednik W, Gheorghita-Baechler F, Dubois R, Guernsey DL, Van der Loos H, Neumann PE. Altered sensory processing in the somatosensory cortex of the mouse mutant barrelless. Science. 1996; 271(5257):1864–1867. [PubMed: 8596955]

Weller WL. SmI cortical barrels in an Australian marsupial, Trichosurus vulpecula (brush-tailed possum): structural organization, patterned distribution, and somatotopic relationships. J Comp Neurol. 1993; 337(3):471–492. [PubMed: 8282853]

Wong P, Kaas JH. An architectonic study of the neocortex of the short-tailed opossum (Monodelphis domestica). Brain Behav Evol. 2009; 73(3):206–228. [PubMed: 19546531]

Wong-Riley MT, Welt C. Histochemical changes in cytochrome oxidase of cortical barrels after vibrissal removal in neonatal and adult mice. Proceedings of the National Academy of Sciences of the United States of America. 1980; 77(4):2333–2337. [PubMed: 6246540]

Wong-Riley MTT. Cytochrome oxidase: an endogenous metabolic marker for neuronal activity. Trends in Neurosciences. 1989; 12(3):94–101. [PubMed: 2469224]

Woolsey TA, Van der Loos H. The structural organization of layer IV in the somatosensory region (SI) of mouse cerebral cortex. The description of a cortical field composed of discrete cytoarchitectonic units. Brain Res. 1970; 17(2):205–242. [PubMed: 4904874]

Woolsey TA, Welker C, Schwartz RH. Comparative anatomical studies of the SmL face cortex with special reference to the occurrence of “barrels” in layer IV. J Comp Neurol. 1975; 164(1):79–94. [PubMed: 809494]

Yang Z, Seif I, Armstrong-James M. Differences in Somatosensory Processing in S1 Barrel Cortex between Normal and Monoamine Oxidase A Knockout (Tg8) Adult Mice. Cerebral Cortex. 2001; 11(1):26–36. [PubMed: 11113033]

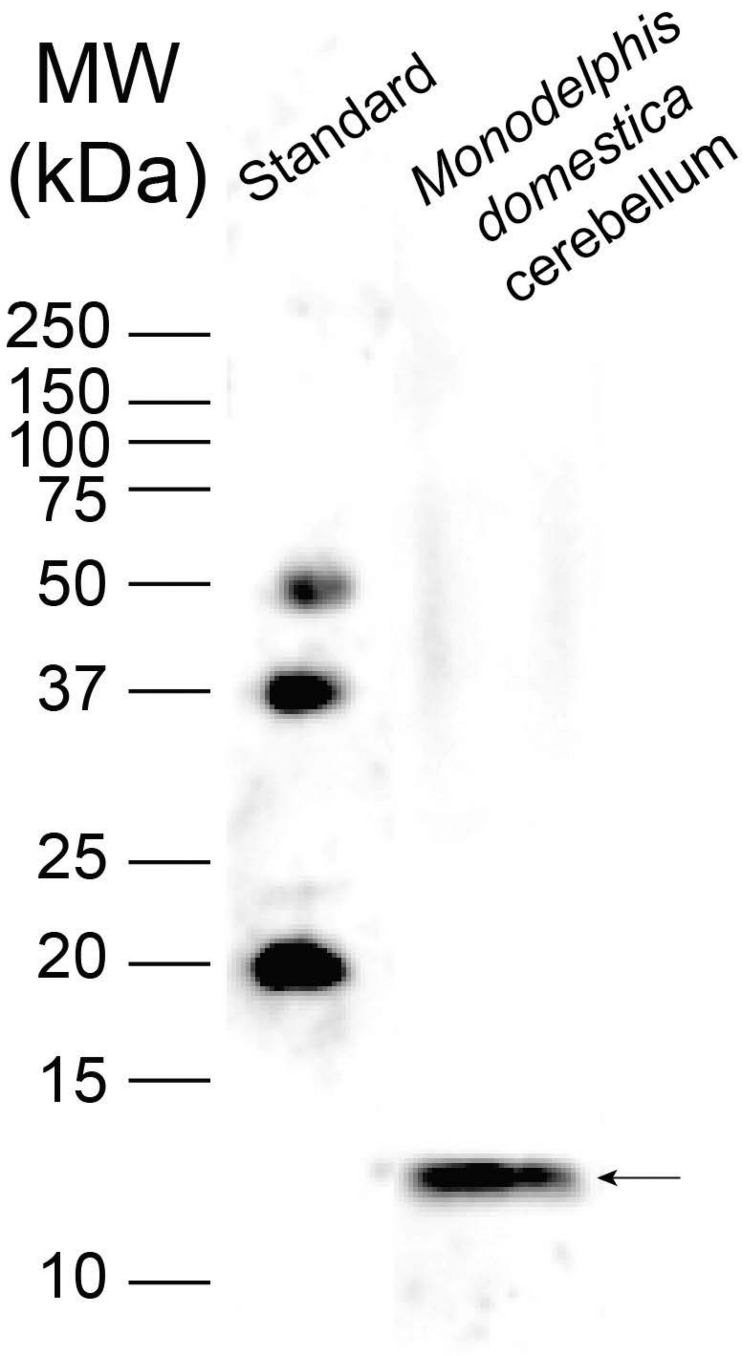

Figure 1.
Western blot characterization of the anti-parvalbumin antibody. A single protein band (arrow) is detected at 12–13 kDa in short-tailed opossum cerebellar lysate; this is within the expected molecular weight range of the parvalbumin protein.

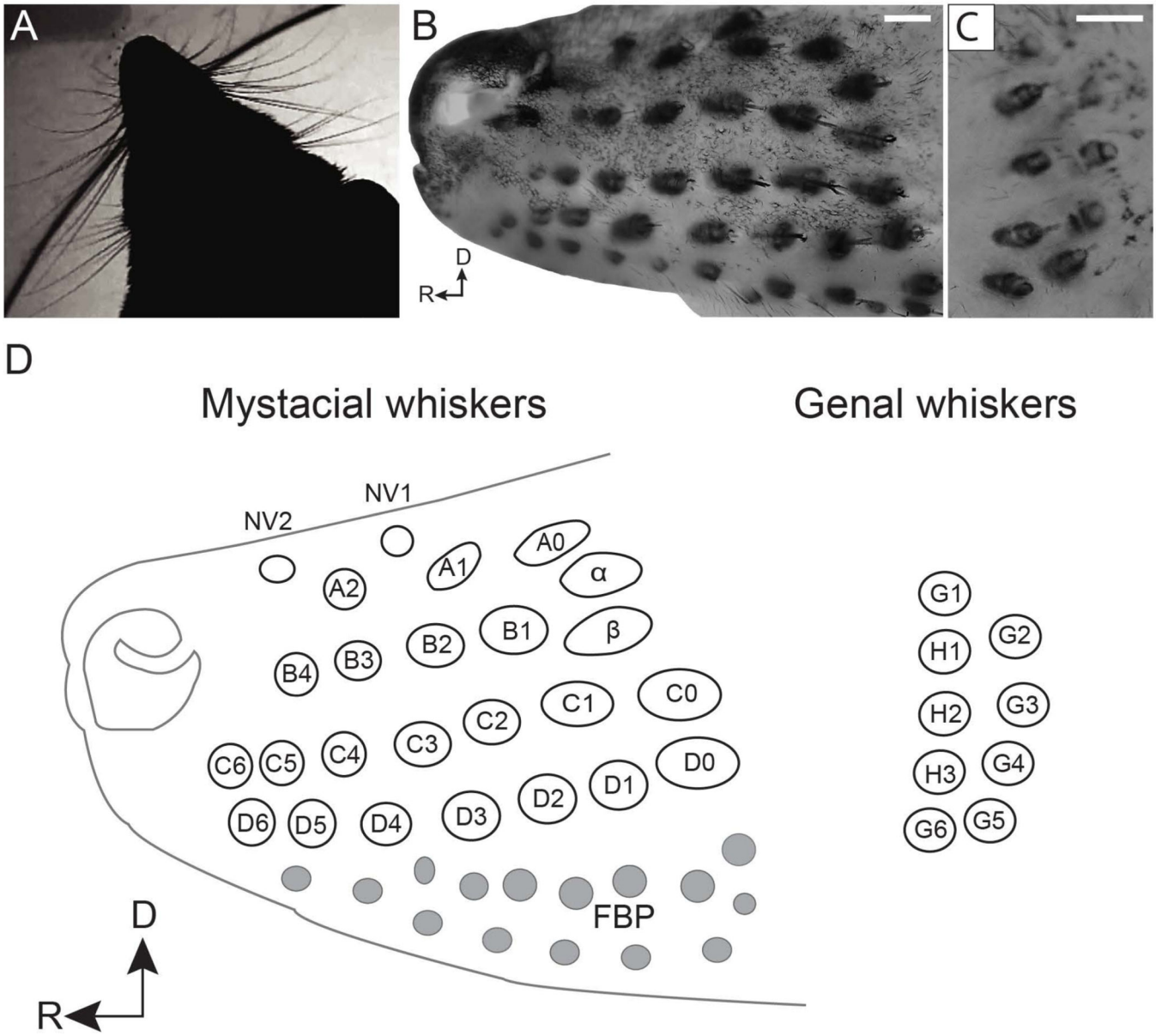

Figure 2.

The arrangement of the large facial whiskers in *Monodelphis domestica*. **A**. A dorsal view of a whisking short-tailed opossum in silhouette shows the position of the mystacial whiskers on the snout, and the genal whiskers on the cheeks. Supraorbital, submental and interramal whiskers are also present in short-tailed opossums, but were not studied in the current work. **B**. Mystacial whisker follicles revealed in an ethanol/xylene cleared preparation of the mystacial pad. Scale bar = 2 mm. Dorsal (D) and rostral (R) directions are indicated by arrows. **C**. Whisker follicles revealed in an ethanol/xylene cleared preparation of the genal pad. Scale bar = 2 mm. **D**. A schematic illustration of the whisker pad in *Monodelphis domestica* (adapted from Grant et al., 2013). Twenty-three mystacial whiskers are named after their row (A–D) and arc (0–6) position, and are highly stereotyped in their number and location, with 3–7 whiskers in each row. Two straddler whiskers are present, α and β. Nasal

whiskers (NV1-2) are found dorsal to the mystacial pad. The furry buccal pad (FBP) is located ventral to the mystacial pad. Unlike the mystacial whiskers, the number of genal whiskers is variable, with five to ten located caudal to the mystacial pad, arranged in vertical groups with 1–2 arcs (G–H); they are named after the arc in which they are located, and their numeric position within the arc (1 being the most dorsal). Dorsal (D) and rostral (R) directions are indicated by arrows.

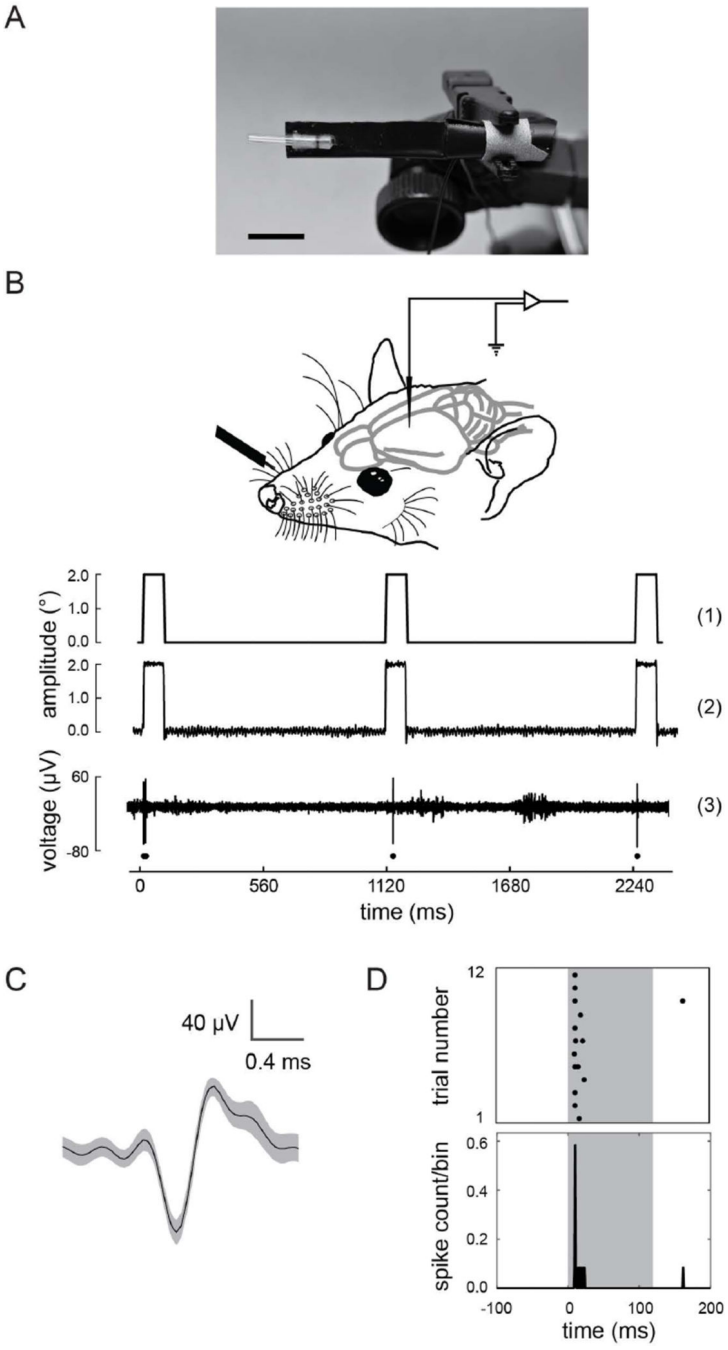

Figure 3.

Experimental design. **A**. A photograph showing the piezoelectric whisker stimulator. Scale bar = 10 mm. **B**. Schematic showing the electrophysiological recording set-up. Trace (**1**) shows the computer-generated ramp-hold-return signal (10 ms ramp, 100 ms hold, 10 ms return) on 3 consecutive trials. Trace (**2**) shows the movement of a whisker using the piezoelectric device, calibrated using a photodetector circuit. Trace (**3**) shows extracellular activity recorded from somatosensory cortex in response to the deflection of an individual whisker on the contralateral face using the computer-controlled piezoelectric device. Spikes

evoked in response to whisker deflection in a single neuron are indicated by black dots beneath the voltage trace. **C**. Average spike waveform for the neuron shown in (B) indicates good single unit isolation. The gray shaded region represents the standard deviation of the mean. **D**. Raster plot and peristimulus time histogram obtained for the neuron (same as shown in (B) and (C)) across 12 trials. The shaded region indicates the duration of the stimulus.

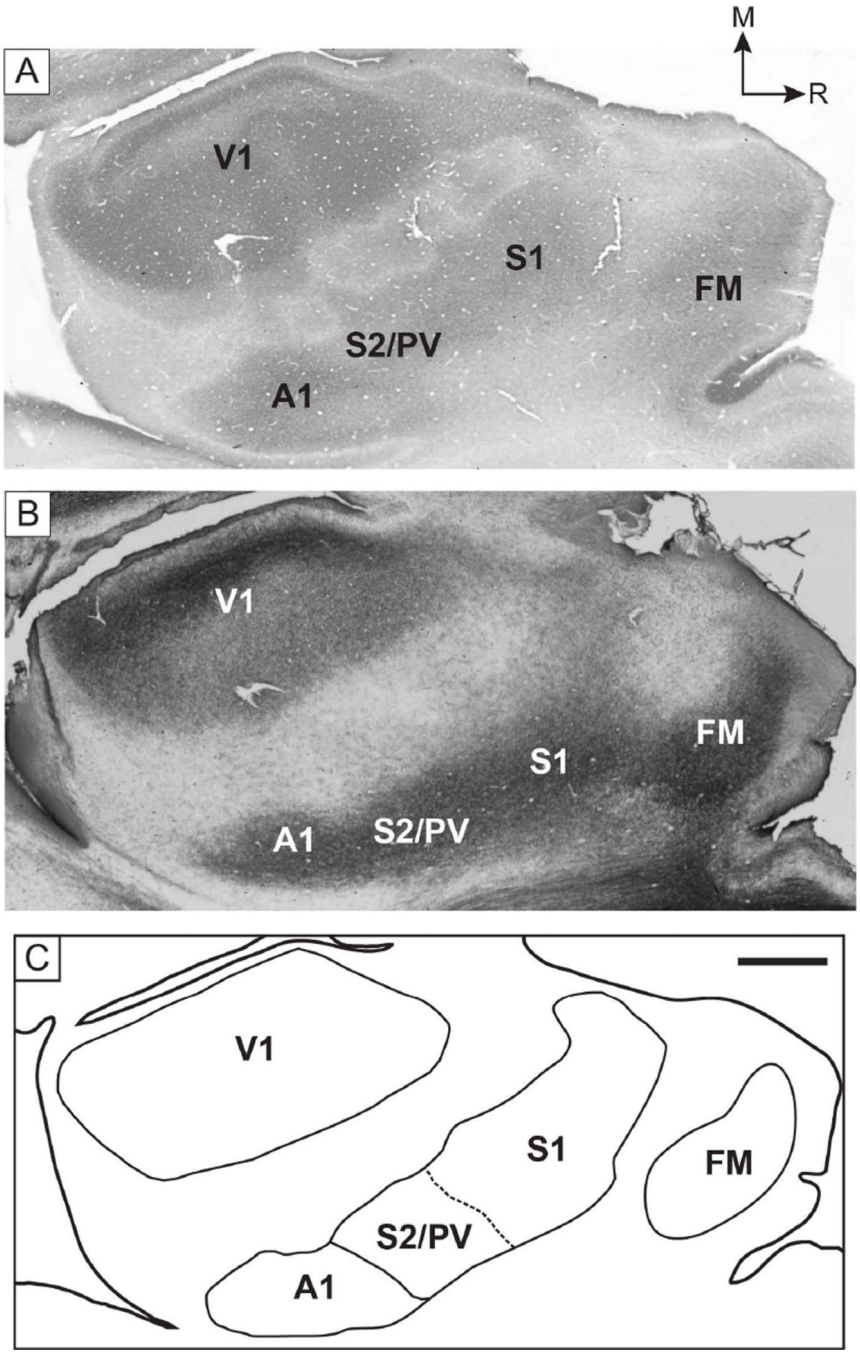

Figure 4.

Architectural boundaries of S1 and surrounding cortex. **A**. Cytochrome oxidase stain of a tangential section of the neocortex. Regions of the cortex that stained dark with cytochrome oxidase were in alignment with densely myelinated regions of the cortex (**B**), including primary sensory areas. Cytochrome oxidase staining within S1 is uniformly dark; no whisker-related patterns are identifiable. **C**. A reconstruction of architectural boundaries drawn from an entire series of sections. Scale bar = 1 mm. Medial (M) and rostral (R) directions are indicated by arrows, and apply to all panels. See Table 1 for abbreviations.

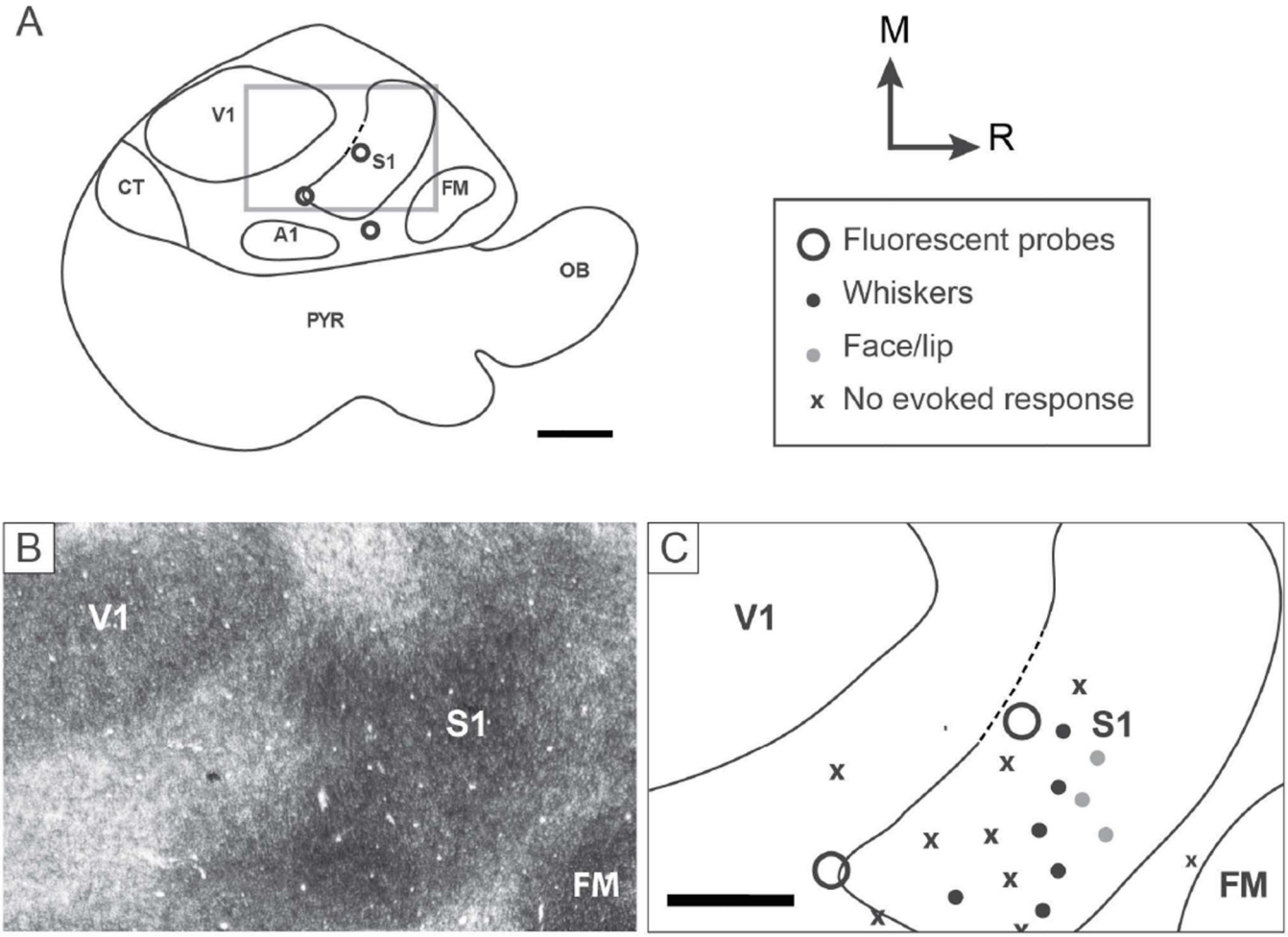

Figure 5.

The relation of electrophysiological recording sites to architectonically determined borders of S1. **A**. A reconstruction of myeloarchitectural boundaries on a tangential section of the cortex. These boundaries were drawn from an entire series of sections. The location of fiducial probes is indicated by open circles and the regions corresponding to images in (**B**) and (**C**) are outlined by the gray square. Scale bar = 2 mm. Medial (M) and rostral (R) directions are indicated by arrows, and apply to all panels. See Table 1 for abbreviations. **B**. A myelin stain of the boxed region in the tangential section shown in (**A**), and the location of electrode penetrations (**C**) relative to architectural boundaries of the primary somatosensory cortex for the section show in (**B**). S1 is readily distinguished from adjacent cortex by its dark myelination. Scale bar = 1 mm.

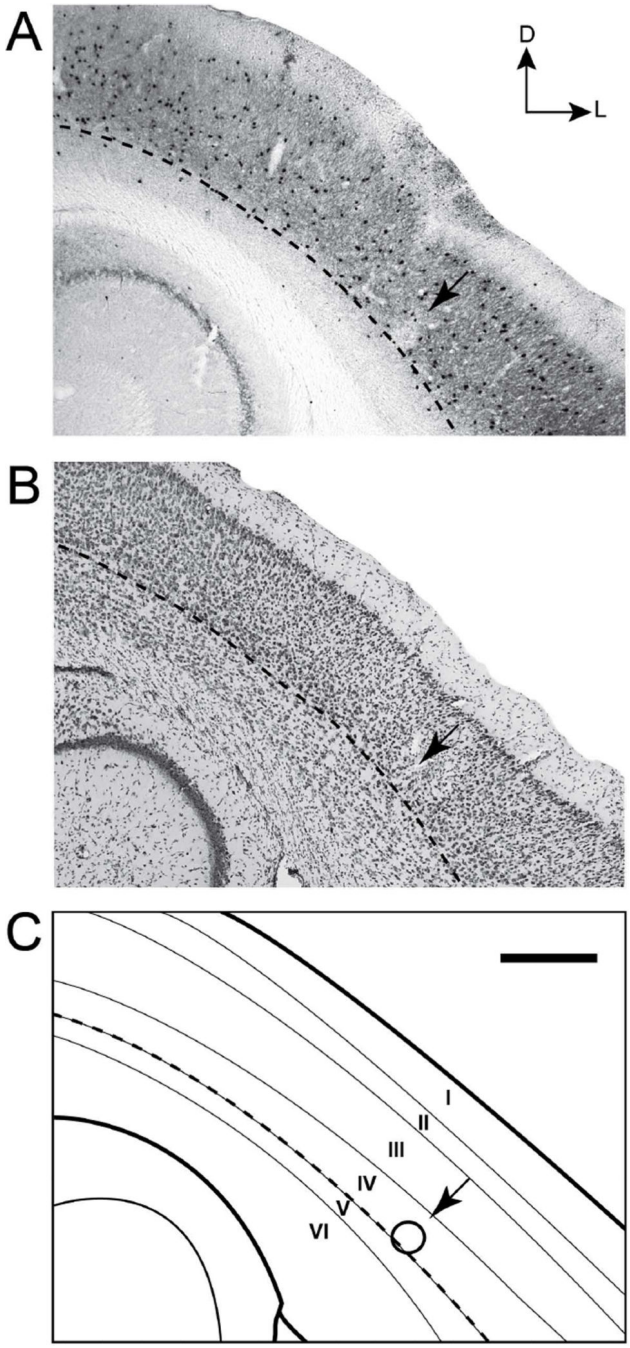

Figure 6.

The relation of electrophysiological recording sites to laminar borders of S1. Coronal sections of the brain stained for parvalbumin (**A**) and Nissl (**B**) with an electrolytic lesion made at a recording site (indicated by the arrow), visible in layer IV of the cortex (**B**). Dorsal (D) and lateral (L) directions are indicated by arrows, and apply to all panels. **C**. A reconstruction of laminar boundaries from these coronal sections of the cortex with the location of the electrolytic lesion indicated by the black circle. The dashed line in (**A**), (**B**) and (**C**) marks the ventral boundary of layer IV. Scale bar = 250 μm.

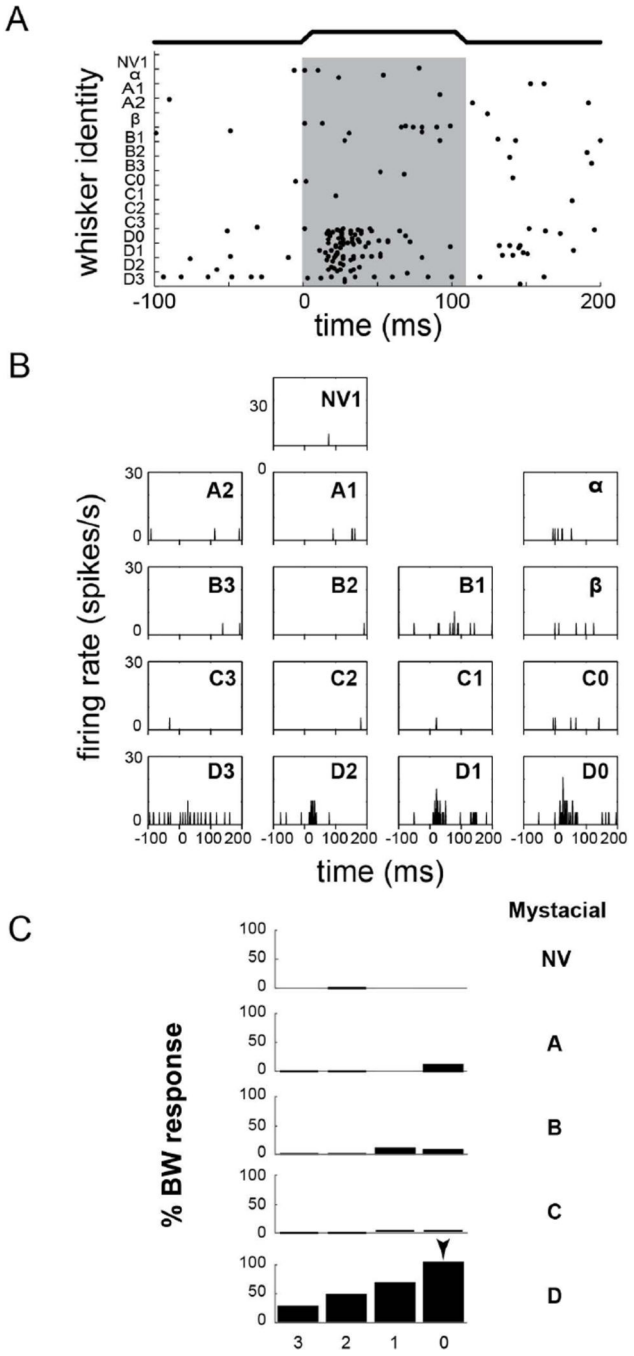

Figure 7.

Responses of a single neuron in S1 with a receptive field on the mystacial whiskers. **A**. A spike raster plot for a neuron in S1 in response to the stimulation of 16 individual mystacial whiskers. The shaded region denotes the duration of the stimulus. **B**. Peristimulus time histograms of the same neuron in response to the deflection of the different mystacial whiskers. **C**. The magnitude of the neuronal response (integrated spike count, 0–75 ms) to each whisker, visualized as a percentage of the best whisker response. The best whisker, D0, is indicated with an arrow.

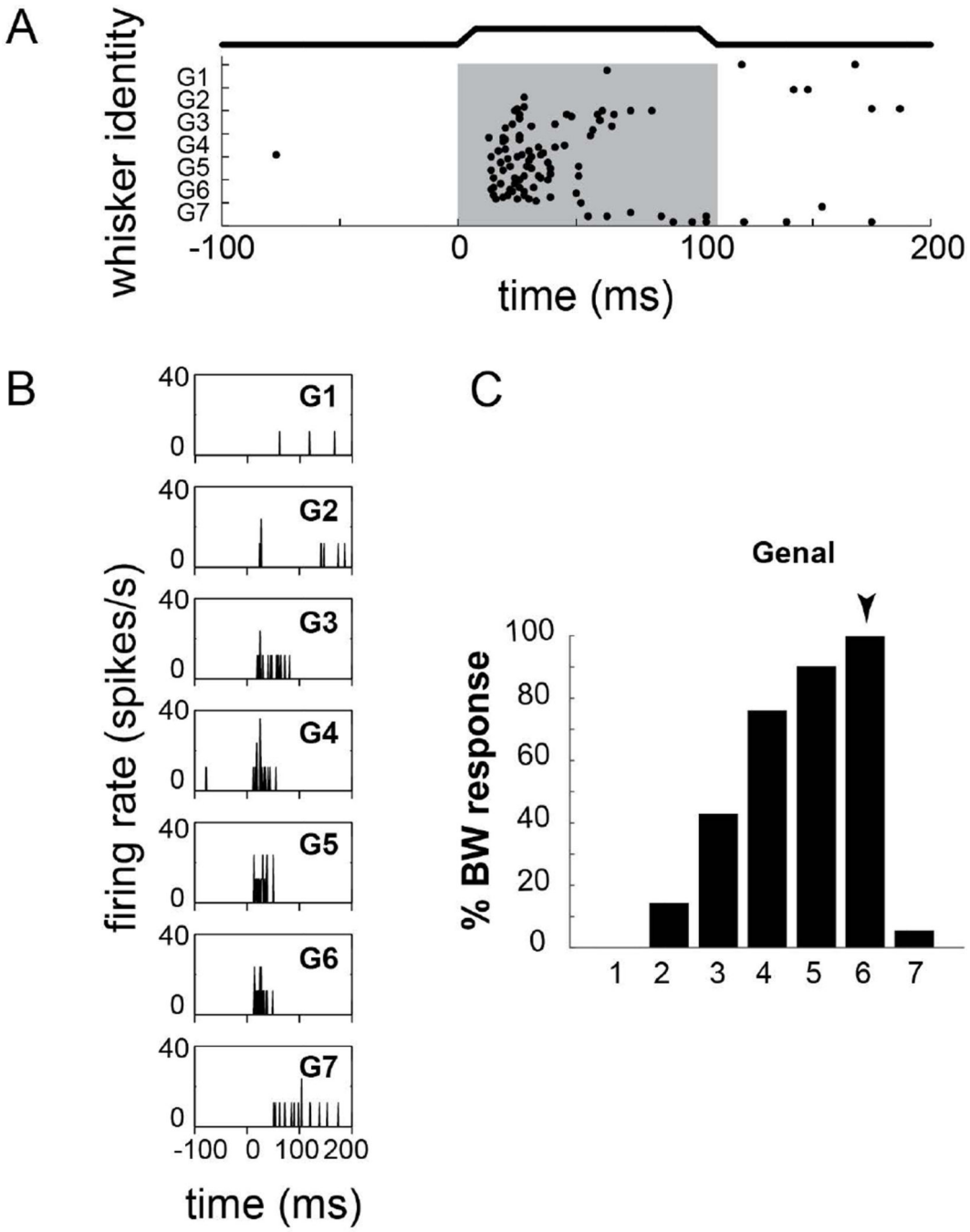

Figure 8.

Responses of a single neuron in S1 with a receptive field on the genal whiskers. **A**. A spike raster plot for a neuron in S1 in response to the stimulation of 7 individual genal whiskers. The shaded region indicates the duration of the stimulus. **B**. Peristimulus time histograms of the same neuron in response to the deflection of the different genal whiskers. **C**. The magnitude of the neuronal response (integrated spike count, 0–75 ms) to each whisker, visualized as a percentage of the best whisker response. The best whisker, G6, is indicated with an arrow.

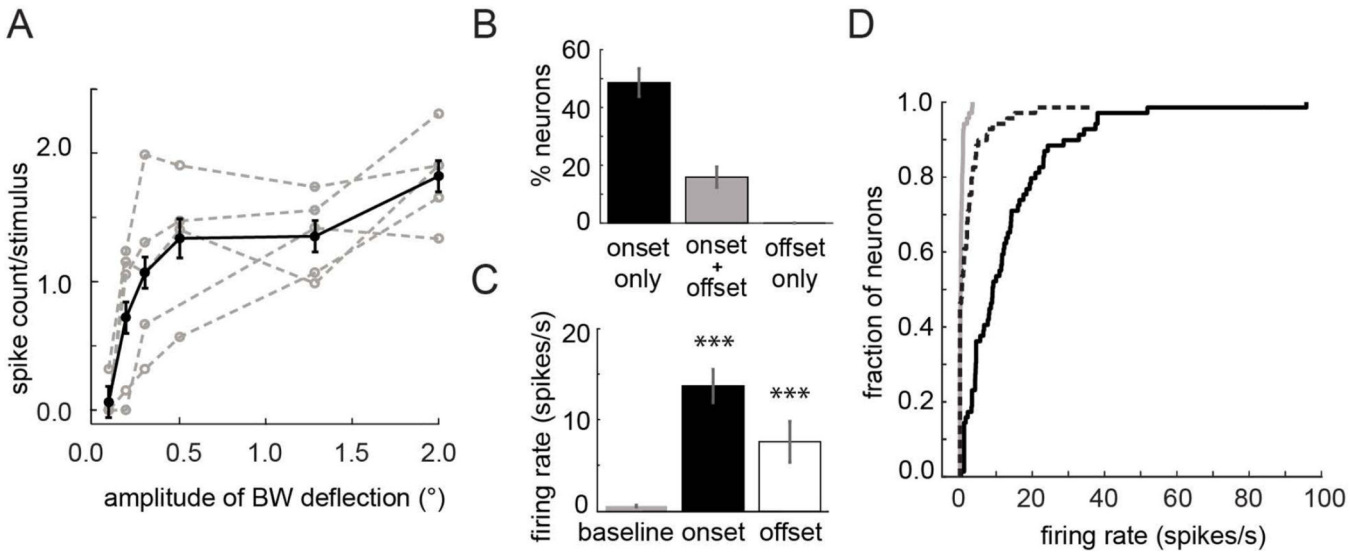

Figure 9.

Summary of spontaneous and evoked firing rates. **A**. Mean stimulus strength-response function for five different layer IV neurons (black), plotted for incremental deflections (0.1–2.0°) applied to the best whisker (BW). Response functions for the individual neurons are also shown (gray, dotted lines). Stimuli were applied at distance of 5 mm from the face. Response magnitudes were measured as spike counts 0–75 ms following stimulus onset, averaged across trials (12, 25 or 50). **B**. Percentages of recorded units (n = 107) that display a significant response to stimulus onset only (black bar – 49%), both stimulus onset and offset (gray bar – 17%) and stimulus offset (white bar – 0%). Error bars show standard error of the proportion. **C**. Comparison of the mean prestimulus spontaneous firing rate (gray bar), and evoked firing rates during the onset period (black bar) and the offset period (white bar). Error bars show standard error of the mean. The asterisks denote significant differences of onset and offset firing rates relative to spontaneous activity (two-sample t-test, $p<0.001$; Wilcoxon rank sum test, $p<0.001$). **D**. Cumulative distributions of spontaneous (gray line), onset (black line), and offset period (dashed line) firing rates for the neurons included in receptive field analyses (onset responsive neurons, n = 70). Spontaneous firing rates were low. Onset and offset spike counts were measured in a 75 ms time window following stimulus onset and offset, respectively, and were considered to be significant if they exceeded two standard deviations above the spontaneous spike count in a 75 ms prestimulus window. Analysis of spatial and temporal response characteristics was performed only for onset responses, in the current study.

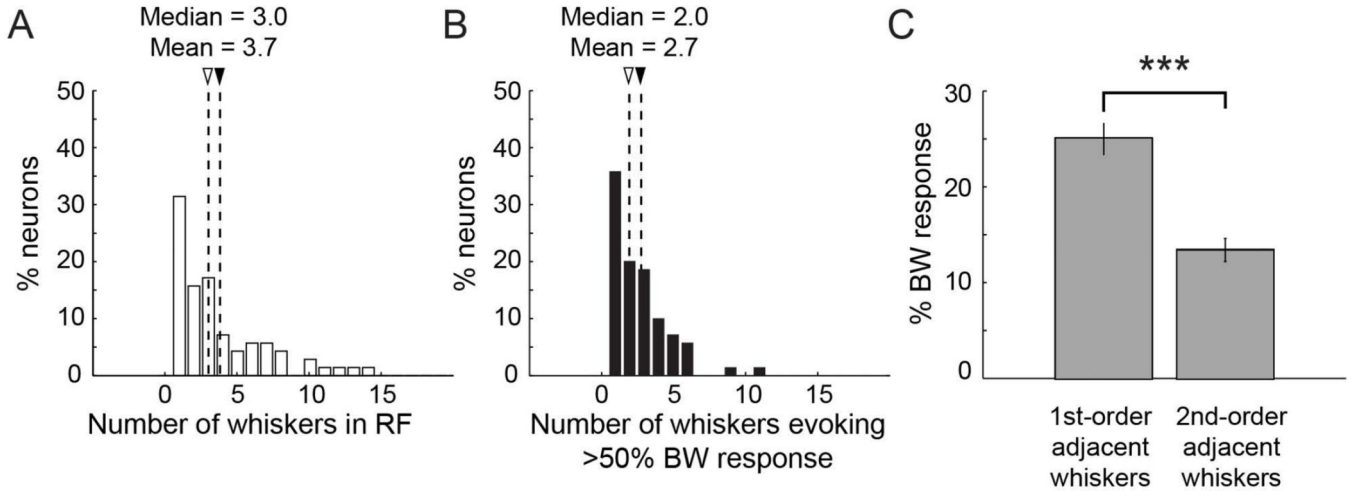

Figure 10.

Summary of receptive field sizes. **A**. The distribution of receptive field sizes of single neurons, measured as the number of whiskers that evoke a significant response above spontaneous activity. Among responsive S1 neurons (n=70), 31% responded only to a single whisker; the remaining 69% of neurons displayed multiwhisker receptive fields. **B**. The distribution of the number of whiskers in each receptive field evoking a response greater than 50% of the best whisker (BW) response. For 64% of neurons, more than one whisker elicited a response greater than half the magnitude of the best whisker response. White arrows indicate median values, black arrows indicate mean values. **C**. Comparison of the mean response magnitude (relative to the best whisker) of first-order adjacent whiskers and second-order adjacent whiskers. Error bars show standard error of the mean. There was a significant decrease in the magnitude of the neural response between the first-order and second-order adjacent whiskers (two-sample t-test, $p<0.001$; Wilcoxon rank sum test, $p<0.001$).

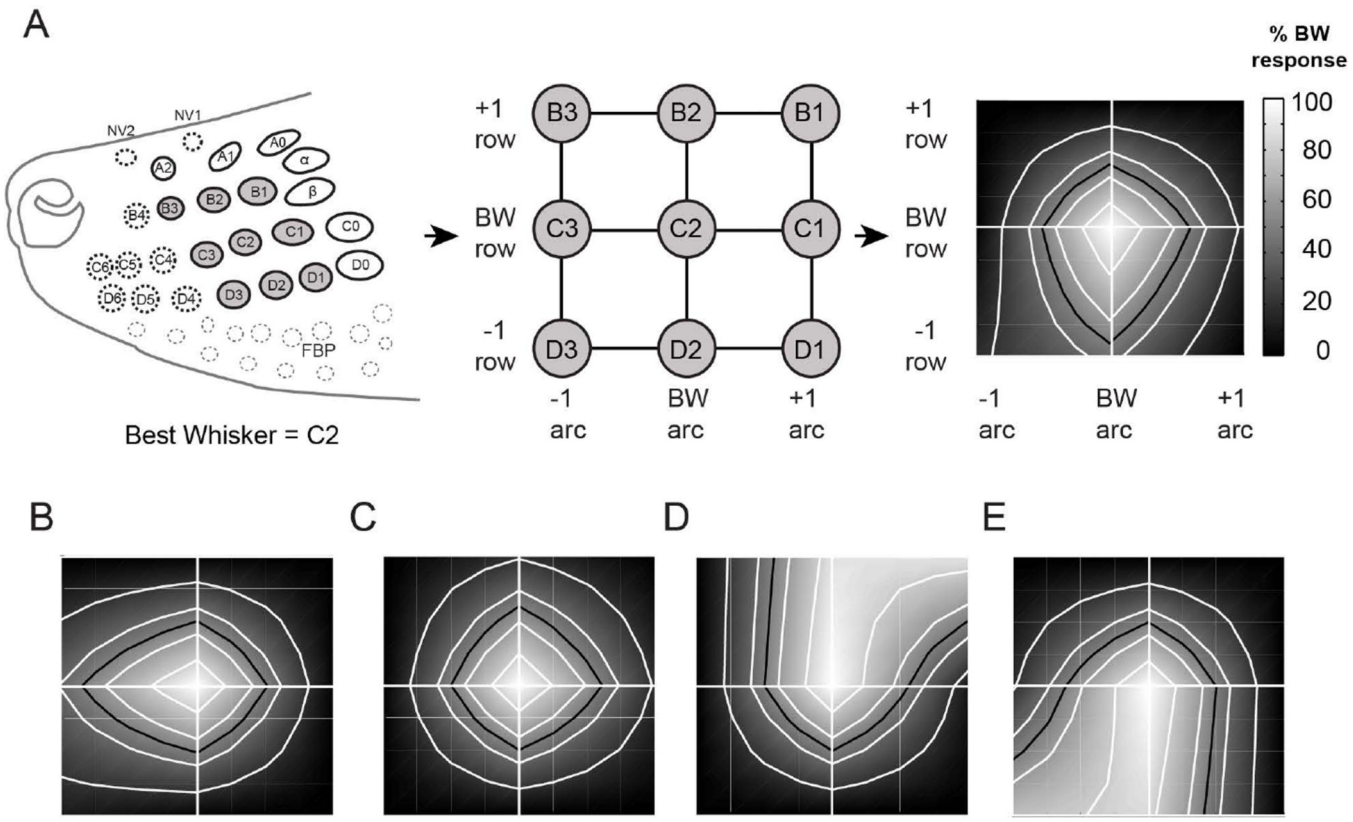

Figure 11.

The receptive field configuration of single neurons in S1. **A**. A visualization of the receptive field of an example neuron, with C2 as the best whisker. On the left is an illustration of the mystacial pad. All tested whiskers are encircled using solid lines, while untested whiskers are indicated using dashed lines. The best whisker and 8 immediately surrounding whiskers for this example are indicated by the gray fill. In the center is a schematic representation of the best whisker and 8 surrounding whiskers as a 3×3 grid. On the right is the contour plot obtained using the response magnitudes to the stimulation of each of the whiskers in the 3×3 grid. The spatial configuration of the receptive field was examined by considering the response magnitude of the best whisker (center of the receptive field) and the 8 immediately adjacent surrounding whiskers. White contour lines show 20, 40, 60, and 80% response levels (relative to the best whisker). Black contour lines show the 50% response level (half height of the two-dimensional tuning curve). **B–E**. Examples of contour plots of the receptive fields for four additional neurons. While we observed different shapes of receptive fields (e.g. D and E), the most common receptive field shape was oval or round.

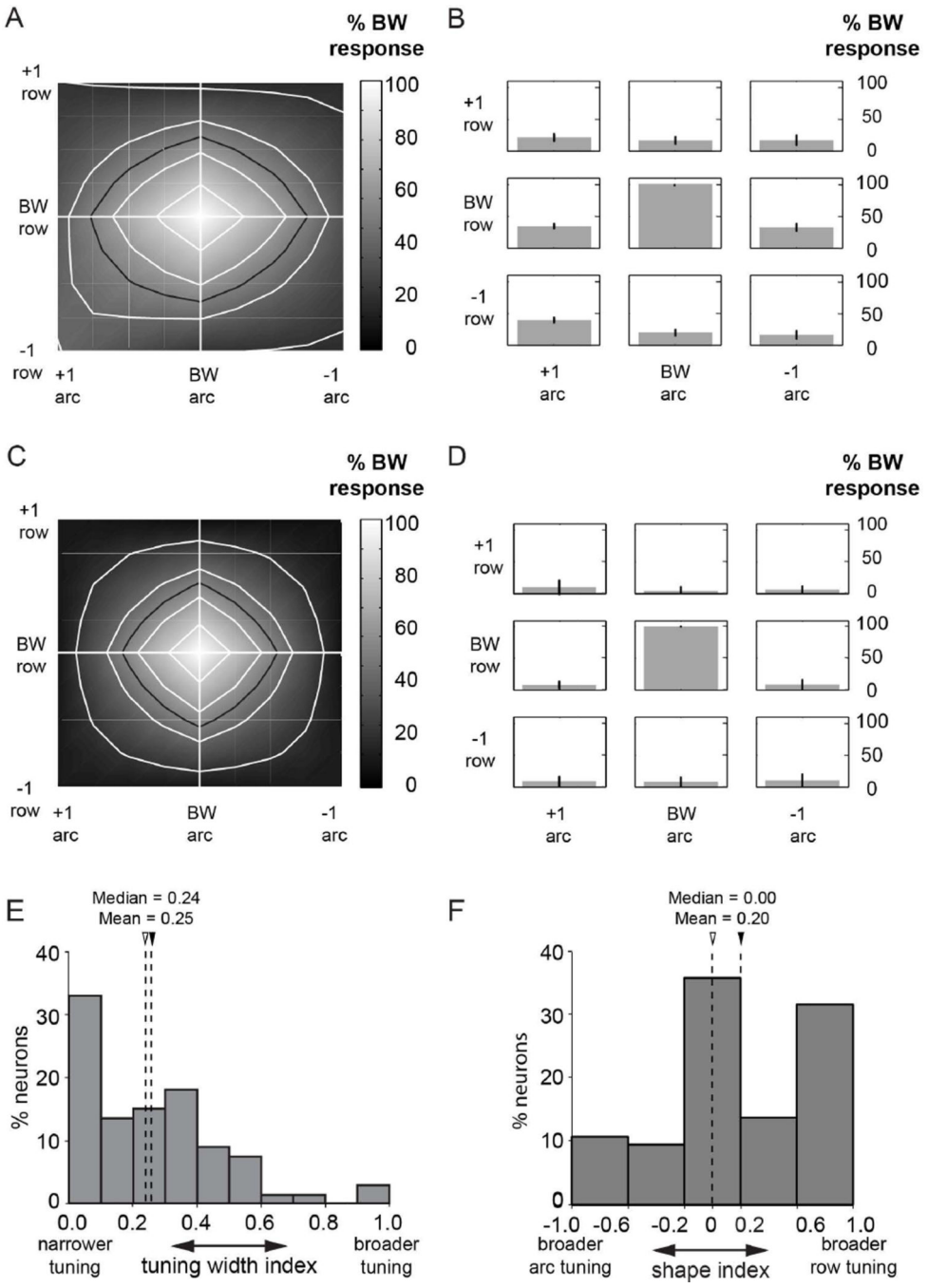

Figure 12.

Mean receptive field configuration. **A**. Average single neuron receptive field (n = 70). The contour plot is centered on the best whisker (BW). **B**. Data in (**A**) visualized using a bar chart; error bars show standard error of the mean. **C**. Average single neuron receptive field contour plot including only neurons for which whiskers were present at all 8 positions surrounding the best whisker (n =7). **D**. Data in (**C**) visualized using a bar chart; error bars show standard error of the mean. **E**. Tuning width index distribution for the whole dataset. Higher tuning width index values indicate broader receptive fields. **F**. Shape index

distribution for the whole dataset. Positive values indicate broader tuning along the row of the best whisker, and negative values indicate broader tuning along the arc of the best whisker. White arrows indicate median values, black arrows indicate mean values.

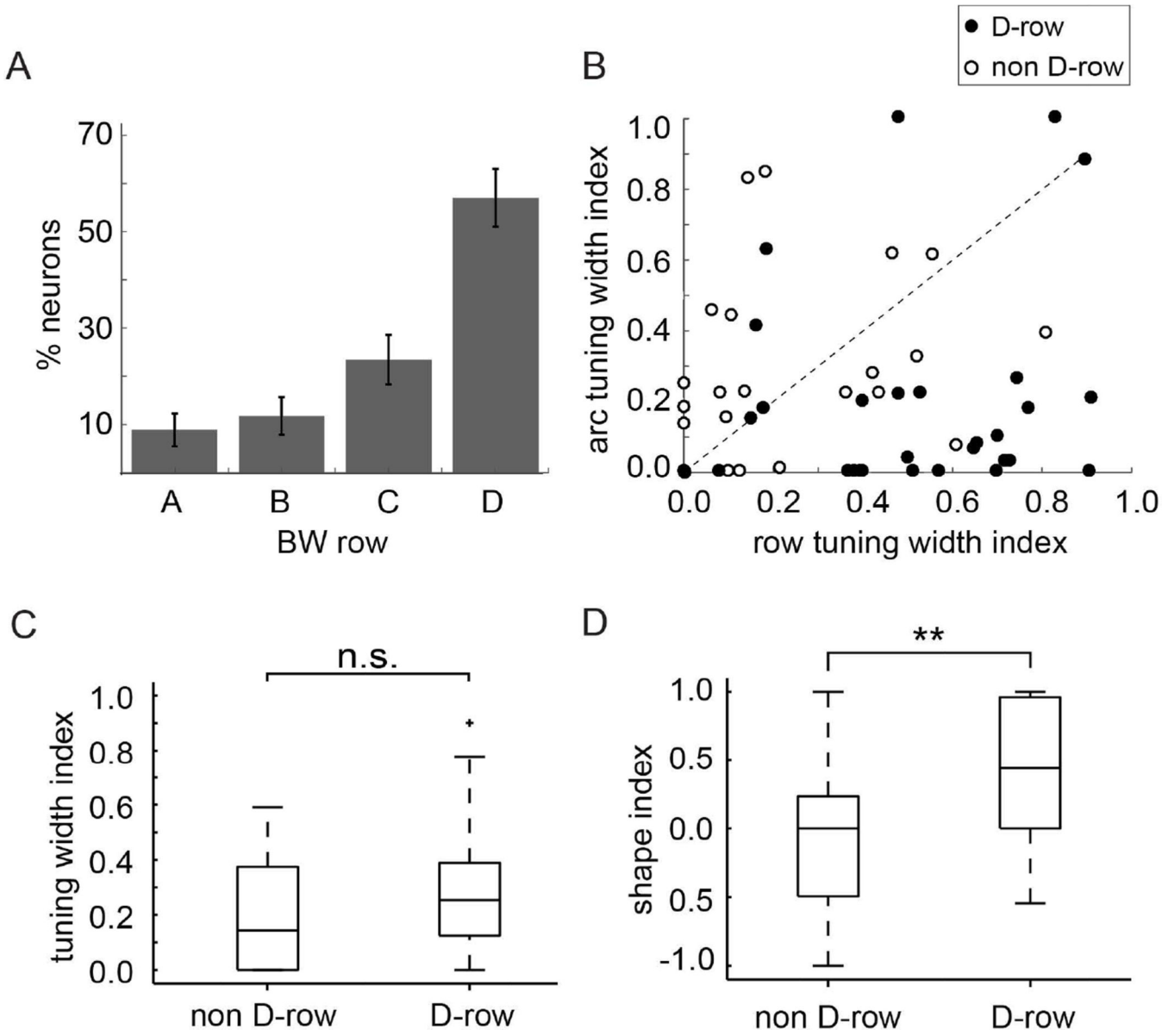

Figure 13.

Tuning differences based on best whisker position. **A**. Distribution of best whisker (BW) positions for the dataset of neurons in S1 that showed the greatest magnitude of response to the deflection of a mystacial whisker. Error bars show standard error of the proportion. Our dataset was dominated by neurons that had their best whisker in the D-row (57% D-row, in comparison to 43% all non D-row whiskers). **B**. Scatterplot showing the relationship between the row tuning width index and arc tuning width index for individual neurons in S1. Neurons that had their best whisker in non D-rows (A, B, C rows) are denoted by white circles while neurons that had their best whisker in the D-row are denoted by black circles. Receptive fields for neurons with D-row best whiskers usually had higher row tuning width indices compared to arc tuning width indices, while the opposite was true for neurons with non D-row best whiskers, suggesting that the D-row group was more broadly tuned along

the best whisker row and the non D-row group was more broadly tuned along the best whisker arc. **C**. Box plots comparing the tuning width indices of D-row and non D-row groups. Surrounding whiskers in both the D-row group and the non D-row group evoked a similar level of responsiveness relative to the best whisker (Wilcoxon rank sum test, $p>0.05$). **D**. Box plots comparing the shape indices of D-row and non D-row groups. The median shape index of the D-row group of neurons was significantly higher than that of non D-row neurons (Wilcoxon rank sum test, $p<0.01$), indicating that although the relative response magnitude to the surrounding whiskers is comparable in the D-row and non D-row groups, as shown in (**C**), the surround response is more skewed along the best whisker row, rather than the best whisker arc, for the D-row group of neurons.

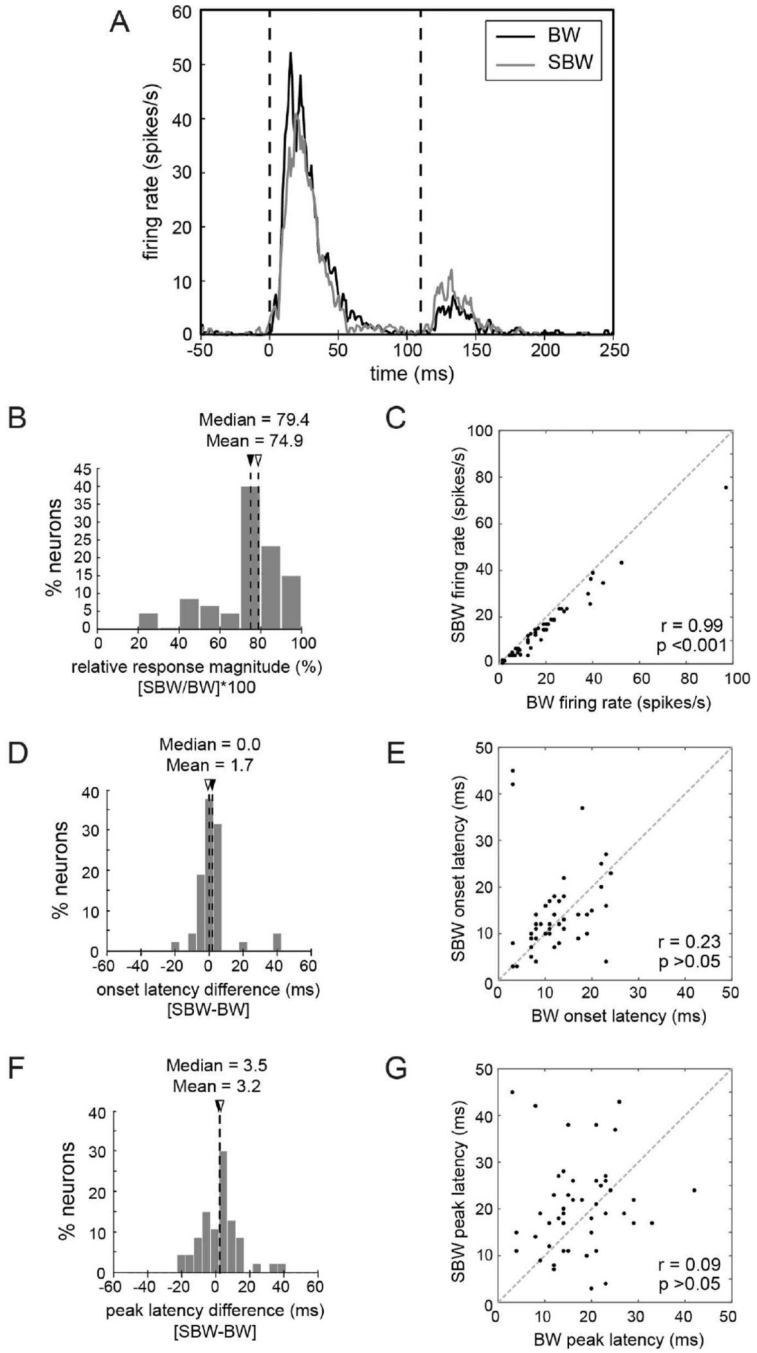

Figure 14.

Temporal response characteristics of single neurons in S1. **A**: Population average PSTHs in response to the deflection of the BW (black line) and the SBW (gray line). Dashed lines indicate stimulus onset and offset. **B**: Distribution of the relative response magnitude to SBW deflection. Distribution for the entire data set is skewed toward the BW response (100%; mean: 74.9 ± 2%, solid arrowhead; median 79.4% ± 3%, open arrowhead), indicating that, in most cases, the SBW evoked high-magnitude responses that were close to the value of the BW response. **C**: Scatterplot showing the relationship between the onset

period firing rates following BW and SBW deflection; same data as in **A, B**. Although the deflection of the SBW evoked a firing rate close to the response evoked by the BW, the median difference in the magnitude of the responses to the BW and the SBW was significantly greater than 0 ($P < 0.001$, Wilcoxon signed-rank test). **D**: Distribution of the differences in the onset latencies of BW and SBW evoked responses. Distribution for the entire data set peaks at approximately 0 msec (mean 1.7 ± 1.4 msec, solid arrowhead; median 0.0 ± 1.7 msec, open arrowhead), suggesting that there is little difference in the onset latencies of the responses to the BW and the SBW. **E**: Scatterplot showing the relationship between the onset latencies of the neural responses following BW and SBW deflection; same data as in **A, C**. The median difference in the onset latencies of the responses to the BW and the SBW was not significantly different from 0 ($P > 0.05$ Wilcoxon signed-rank test). **F**: Distribution of the differences in the peak latencies BW and SBW evoked responses. Distribution was slightly skewed toward positive values (mean 3.2 ± 1.7 msec, solid arrowhead; median 3.5 ± 2.1 msec, open arrowhead), suggesting that there was only a small trend for the BW peak latency to precede the SBW peak latency. **G**: Scatterplot showing the relationship between the peak latencies of the neural responses following BW and SBW deflection; same data as in **A, F**. The median difference in the peak latencies of the responses to the BW and the SBW was not significantly different from 0 ($P > 0.05$ Wilcoxon signed-rank test).

Table 1

Abbreviations

3b	Primary somatosensory cortex
A1	Primary auditory cortex
BW	Best whisker
CT	Caudal temporal area
FBP	Furry buccal pad
FM	Frontal myelinated area
IM	Intramuscular
IP	Intraperitoneal
ISI	Interspike interval
OB	Olfactory bulb
PSTH	Peristimulus time histogram
PV	Parietal ventral area
PYR	Piriform cortex
RF	Receptive field
S1	Primary somatosensory cortex
S2	Secondary somatosensory cortex
SBW	Second best whisker
V1	Primary visual cortex

Table 2

Antibody Characterization

Antigen	Immunogen	Manufacturer	Dilution factor
Parvalbumin	Purified frog muscle parvalbumin	Sigma-Aldrich Cat# P3088, RRID:AB_477329; Mouse monoclonal anti-parvalbumin	1:2000

Table 3

Best whisker of single neurons recorded per penetration

Penetrations	Animals							
	A	**B**	**C**	**D**	**E**	**F**	**G**	**H**
1	A2	A1	α	B1	A2	C3	D3	G6
2	A1,B3	B2	B3	C0	C3,C3,C3	C3, C3,D3		
3	α,B2	C4,C4, D5	B2,B2	C1	C2	C1, D2,D0		
4		C4,D4	B1	D3,D3, D2,D3	C2,D3	C0,D1		
5		D1,D1	C2	D2, D2	D3,D3	D3		
6			D2	D1,D1	D1,D1	D3		
7				D1	D1,D1, D3	D3		
8					D1,D2	D3		
9					D0	D2		
10						D1		
11						D1		
12						D1		
13						D0		

The table shows a summary of the sampling of neurons that displayed a significant response to the deflection of at least one whisker (70/107). Each column of the table lists the recording penetrations (1–13) for an individual animal (Opossum A–H). In one animal (Opossum I), no neurons were found to evoke a significant response as per our criteria (see *Methods*), and therefore this experiment does not show up in the table. For each penetration, the identity of the best whisker of each neuron analyzed per penetration is listed.

Table 4

Summary of neural response magnitudes and latencies for BW and SBW deflection

	Response magnitude (spikes/stimulus)				Onset latency (ms)				Peak latency (ms)			
	BW		SBW		BW		SBW		BW		SBW	
	Mean	Median	Mean	Median	Mean	Median	Mean	Median	Mean	Median	Mean	Median
10 ms ramp n = 48	1.42 ± 0.18	1.17 ± 0.22	1.12 ± 0.15	0.94 ± 0.19	12.0 ± 0.88	11.5 ± 1.11	13.8 ± 1.32	12.0 ± 1.66	17.3 ± 1.12	15.5 ± 1.40	20.5 ± 1.42	19.0 ± 1.78
4 ms ramp n = 16	1.41 ± 0.17	1.24 ± 0.21	1.20 ± 0.16	1.12 ± 0.21	9.84 ± 2.02	7.00 ± 2.53	11.4 ± 3.11	7.00 ± 3.89	17.5 ± 3.10	13.0 ± 3.89	18.0 ± 3.62	14.0 ± 4.54